ANSTO/E684

ANSTO/E684

THE AUSTRALIAN COMMONWEALTH STANDARD OF MEASUREMENT FOR ABSORBED RADIATION DOSE

PART 1: CONTROL, MONITORING AND PERFORMANCE OF THE URQUHART GRAPHITE MICROCALORIMETER

by

S L SHERLOCK

ISSN 1030-7745
ISBN 0 642 59898 3
August 1989

AUSTRALIAN NUCLEAR SCIENCE AND TECHNOLOGY ORGANISATION

LUCAS HEIGHTS RESEARCH LABORATORIES

The Australian Commonwealth Standard of Measurement for Absorbed Radiation Dose

PART 1: Control, Monitoring and Performance of the Urquhart Graphite Microcalorimeter

by

S. L. Sherlock

ABSTRACT

As an agent for the Commonwealth Scientific and Industrial Research Organisation, the Australian Nuclear Science and Technology Organisation is responsible for maintenance of the Australian Commonwealth standard of absorbed dose. This standard of measurement has application in radiation therapy dosimetry, which is required for the treatment of cancer patients.

This report is the first in a series of reports documenting the absorbed dose standard for photon beams in the range from 1 to 25 MeV. The standard has been described previously by Urquhart, Johnson and Badger (1978); however, at that time the standard was maintained for Cobalt-60 energy only.

The graphite calorimeter built by Urquhart et al has been upgraded electronically and subsequently used for absorbed dose measurement under medical linear accelerators installed at Westmead and Royal North Shore hospitals.

The contents of this report are restricted to a consideration of the control, monitoring and performance of the upgraded calorimeter. Later reports describe interpretation of results obtained with the calorimeter, and their application to the determination of absorbed dose in water.

ISSN 1030-7745
ISBN 0 642 59898 3

The following descriptors have been assigned from the INIS Thesaurus to describe the subject content of this report for information retrieval purposes. For further details please refer to IAEA-INIS-12 (INIS: Manual for Indexing) and IAEA-INIS-13 (INIS: Thesaurus) published in Vienna by the International Atomic Energy Agency.

ANSTO; AUSTRALIA; CALIBRATION; CALIBRATION STANDARDS; CALORIMETERS; COBALT 60; DOSIMETRY; GRAPHITE; LINEAR ACCELERATORS; MODIFICATIONS; ON-LINE CONTROL SYSTEMS; ON-LINE MEASUREMENT SYSTEMS; PHANTOMS; PHOTON BEAMS; RESISTORS; RADIATION DOSES; RADIOTHERAPY; SHIELDING; SSDL; TEMPERATURE CONTROL; TEMPERATURE MEASUREMENT; TEMPERATURE MONITORING; VACUUM SYSTEMS.

EDITORIAL NOTE

The Australian Nuclear Science and Technology Organisation (ANSTO) replaced the Australian Atomic Energy Commission (AAEC) on 27 April 1987. Reports issued after April 1987 have the prefix ANSTO with no change of the symbol (E, M, S or C) or numbering sequence.

CONTENTS

1. INTRODUCTION

1.1 The Nature of Absorbed Dose Standards

In the process of radiation absorption, energy lost by ionising radiation is deposited in the medium traversed. The amount of energy thus absorbed by the medium is referred to as "absorbed dose". More precisely absorbed dose is the number of joules per kilogram deposited in the medium.

At the request of the International Commission on Radiation Units (ICRU), the Conférence Générale des Poids et Mesures (CGPM) in 1975 adopted the gray (symbol Gy) as a special name for the joule per kilogram for the measurement of absorbed dose. The gray is thus the SI (Système International d'Unités) unit for absorbed dose.

The National Standards Commission (NSC) was created under the Commonwealth Weights and Measures (National Standards) Act of 1948 (replaced in 1960). This act provided for the establishment and use, throughout Australia, of uniform units and standards of measurement of physical quantities. Under the act, the Commonwealth Scientific and Industrial Research Organisation (CSIRO), is obliged to maintain Australia's primary standards of measurement for all physical quantities for which legal units are prescribed.

In practice, CSIRO maintains the great majority of the primary standards in its Division of Applied Physics. In specialised fields, however, it has appointed agents to maintain the relevant primary standard. In particular, the Australian Nuclear Science and Technology Organisation (ANSTO) maintains the primary standard of measurement for absorbed dose.

At the international level, ANSTO has links with the Bureau International des Poids et Mesures (BIPM). Under the Treaty of the Metre, signed by 17 nations in 1875 (and now adhered to by 46 nations), BIPM was established to maintain the international standards of the metre and the kilogram. To these standards were added, in 1921, electrical units; in 1939 photometric units; and in 1960, units and standards of ionising radiations.

With the exception of the kilogram, none of the base units of the SI system are defined in terms of material objects. At ANSTO, the absorbed dose standard is composed of a measurement instrument, for which an operating procedure is defined. This instrument is a graphite micro-calorimeter.

In view of the limited numbers of laboratories in the world capable of supporting absolute absorbed dose measurement standards, the International Atomic Energy Agency (IAEA), has established a network of laboratories which function to disseminate the standard.

Under this arrangement, the ANSTO laboratory is a designated Secondary Standard Dosimetry Laboratory, or SSDL. Prime responsibility of the laboratory is to verify field dosimeters by calibrating them against secondary standard instruments which are traceable to primary national and/or international standards. In Australia, this means the Lucas Heights laboratory must maintain exposure standards derived from the Australian Radiation Laboratory (ARL).

Under domestic arrangements, the converse is also true. ARL maintain secondary absorbed dose standards derived from the ANSTO primary standard.

A further obligation arises from Australian representation on the committees of the International Organisation of Legal Metrology (OIML). The NSC represents the Australian view in the preparation of OIML international recommendations and international documents which have bearing on legal measurements in this country. An example is the "International document: Secondary standard dosimetry laboratories for the calibration of dosimeters used in radiotherapy" [OIML,1988].

1.2 Relevance to the Community

The principal application of the absorbed dose standard is in the health industry, especially the use of ionising radiation in the treatment of cancer, i.e. radiotherapy. The OIML document [OIML, 1988] states:

'The dosimetry of ionising radiations with high accuracy is essential in order to assure the quality of radiotherapy throughout the world and in order to compare successfully clinical results on an international basis. Similar requirements exist in other related areas of work where radiation is internationally applied, for example in radiobiological studies. This accuracy can only be achieved if calibrated radiation dosimeters are available and checked regularly to maintain acceptable measurement performance'.

Also, the adoption of such SI units as the gray was supported under resolution WHA30.39, adopted by the Thirtieth World Health Assembly in May 1977. This resolution states [WHO, 1977]:

'The Thirtieth World Health Assembly, ...

1. Recommends the adoption of the SI by the entire scientific community, and particularly the medical community throughout the world'.

The practice of radiotherapy is extensive. Very few countries have no radiotherapy treatment centres. In Australia, most major hospitals in the capital cities have Oncology Departments, which include chemotherapy as well as radiotherapy. The treatment machines are mainly linear accelerators, with some Cobalt-60 units still in service. In Australasia in 1987, there were some 50 linear accelerators, 20 Cobalt units and 100 orthovoltage X-ray sets in service. Of the linear accelerators, some 20 were capable of providing electron beams in addition to high energy photon beams.

In all cases, the machines involved must be calibrated for radiation output to allow delivery of the prescribed dose. Further, in Australia, these calibrations must be traceable to Australian standards of measurement.

Errors in dosimetry may lead to underdosing, with the result that the cancer remains uncontrolled; or overdosing, leading to radiation necrosis or early death. The role of the SSDL and standards laboratory is to assist radiation users maintain the calibration of their treatment machines and dosimeters [IAEA, 1987].

1.3 History of AAEC/ANSTO Absorbed Dose Standard

The first effort at establishing an absolute absorbed dose standard was the construction of an aluminium calorimeter [Urquhart, Badger and Johnson 1974]. This was followed by a graphite calorimeter, [Urquhart, Johnson and Badger, 1978], which successfully established an absorbed dose standard for Cobalt-60 gamma rays in graphite.

In 1977, a Nuclear Enterprises NE2560/2561 NPL secondary-standard exposure meter was purchased, subsequently being calibrated against the graphite calorimeter.

During 1985/86, the graphite calorimeter was upgraded, being used in 1986 to re-establish the Cobalt-60 standard. In 1987, the calorimeter was taken to Royal North Shore Hospital in Sydney where measurements were made under the Varian Clinac 1800; these measurements are the basis of the 6 and 18 MeV photon beam standards.

Also in 1987, the NE2560 was taken to ARL, where it was calibrated for Cobalt-60 and Cesium-137 gamma rays in terms of exposure.

In 1988, the calorimeter was again taken off-site, this time to Westmead Hospital. Measurements made under the Philips SL25 are the basis of the 25 MeV standard. Also in 1988, the NE2560 exposure meter was modified to provide operation under computer control.

1.4 Requirement for Upgrade of the Urquhart Calorimeter

In early 1985, the decision was made to extend the absorbed dose standard to include beams from linear accelerators with peak bremsstrahlung energies up to 25 MeV [Sherlock, 1986]. This extension to high energy photon beams meant that the graphite calorimeter would be taken to the hospitals and measurements made in a relatively hostile environment.

In particular, it was known that due to patient treatment needs, only limited access was available to the linear accelerators. Since calorimeter measurements involve slow procedure, some form of automatic data logging and control was essential. With the possibility that the calorimeter would be operating in the treatment room while patients were being irradiated, the vacuum system was required to run quietly, and produce neither heat nor oil vapour.

Accordingly, a complete upgrade of the calorimeter systems was performed to allow operation in the hospital.

The existing vacuum system was abandoned and a new system constructed. This featured a direct-drive backing pump with oil-mist eliminator, a diffusion pump with remote water chiller and new vacuum gauges.

The cable harness connecting the calorimeter to the control electronics was replaced with a 10m run to allow for the extra wall thickness required for shielding 25 MV photon beams. Cable terminations were also modified to allow ready assembly.

Existing analogue control circuits were scrapped, the thermistor Wheatstone bridges rebuilt and control algorithms implemented in software.

No modifications were necessary to the calorimeter, other than repair of vacuum leaks and improvements to the internal wiring arrangement.

1.5 Scope of this Report

The adaption of the calorimeter to computer control and its subsequent application form an extensive body of work. Their inclusion under one cover is not advisable, as clarity of exposition will suffer.

Accordingly, this report addresses only those matters concerned with the computer control and monitoring of the calorimeter. Reference to experimental results is made only to enable evaluation of the successful operation of the calorimeter.

Details concerning correction factors, high energy standards and the determination of absorbed dose to water are left to subsequent reports.

2. THEORY OF CALORIMETRY

2.1 The Nature of Calorimetry

The amount of energy present in a bremsstrahlung beam cannot be measured directly. Rather, the beam must interact with a detector, the response of which is an indirect measure of the energy in the photon beam.

In the case of calorimetry, the energy of the photon beam is degraded by the absorption process into heat. The consequent temperature rise in the absorbing body is then in proportion to the energy transferred from the photon beam into the target matter. When the absorbing matter is pure graphite, it is considered that all the electro-magnetic energy absorbed in the material is degraded to heat, i.e. no energy is stored in the graphite as chemical bonds or crystal lattice defects.

With the specific heat of graphite known, and the temperature rise amenable to measurement, the absorbed dose in a fixed mass of graphite is then known in an absolute fashion, i.e. the energy absorbed is measured directly. This is an application of the calorimetry principle.

The temperature rise induced by bremsstrahlung from medical linear accelerators in absorbed dose calorimetry is typically 20 mK for an absorbed dose of 15 Gy in graphite. Accurate measurement of this small temperature rise requires careful design of the calorimeter, both to produce a high degree of temperature stability and to provide adequate resolution.

2.2 Resolution of Temperature Measurement

Medical linear accelerators typically provide a dose rate of 3 $Gy.min^{-1}$. A practical absorbed dose is about 10 Gy. Absorbed dose D in a small mass m due to an amount of energy absorbed E, is

$$D = \frac{E}{m} \tag{1}$$

The temperature rise θ in the mass m of material having specific heat S is

$$\theta = \frac{E}{mS} \tag{2}$$

Substituting (1) in (2),

$$\theta = \frac{D}{S} \tag{3}$$

For graphite having specific heat 730 $J.kg^{-1}.K^{-1}$, the temperature rise for 10 Gy absorbed dose is 13.7×10^{-3} K. A desirable upper limit for the statistical uncertainty of this measurement is 0.1%, suggesting that a resolution of order 10 μK is required.

Temperature measurement in the Urquhart calorimeter is by use of a thermistor in one arm of a Wheatstone bridge. The output in volts of the bridge is then dependent on temperature. In any resistance, thermal energy produces motion of charged particles. This charge movement is called Johnson noise or thermal noise, and the peak-to-peak noise voltage E_{p-p} of a resistor R is given at room temperature by [Keithley, 1984].

$$E_{p-p} = 6.5 \times 10^{-10} \sqrt{R\Delta f} \tag{4}$$

The quantity Δf is the noise bandwidth in Hz, which may be taken as 1 Hz if an analog panel meter is used for readout or one half the conversion rate (readings $.s^{-1}$) of an integrating digital voltmeter. The resistance of the thermistor used in the calorimeter is 2.2 kΩ at room temperature. Using a Keithley 147 nanovoltmeter (analog), the peak-to-peak noise voltage generated by the thermistor is at least 30 nV.

The output sensitivity $\frac{\partial V_{out}}{\partial R_1}$ of a Wheatstone bridge with R_1 the thermistor resistance and R_2 the resistance of the adjacent output arm is

$$\frac{\partial V_{out}}{\partial R_1} = \frac{-R_2}{(R_2+R_1)^2} \text{ Vin} \tag{5}$$

With a 4.05V Mallory mercury cell providing Vin and a value of R_2 of 220 kΩ, the output sensitivity is approximately -20 $\mu V.\Omega^{-1}$. The sensitivity of the thermistor is $-.03\Omega.K^{-1}$, giving a bridge sensitivity of approximately 1300 $\mu V.K^{-1}$. For an absorbed dose of 10 Gy, the bridge output is then 18 μV.

For a resolution of 0.1%, the bridge resolution is required to be 18 nV. With the Johnson noise at least 30 nV, it is apparent that for a single reading of temperature the noise exceeds the resolution required. Thus Johnson noise sets a limit to the resolution of the temperature measurement.

In practice, the noise level problem may be reduced by statistical means. During a calorimeter "run", serial temperature readings are performed during the "drift" and heating periods. By least squares fitting of straight lines to these data, an averaging effect is obtained which increases the resolution.

2.3 Traceability to National Primary Standards

Equation (3) of Section 2.2 suggests that calorimetry is performed by measuring temperature rise θ, determining absorbed dose from the product of θ and the specific heat. In fact, the specific heat may not be known to the desired accuracy; also, the absolute calibration of a thermistor in terms of $\Omega.K^{-1}$ may not be stable.

For this reason, equation (1) is preferred, with the implication that energy E be determined absolutely. Since the absorbing element is provided with a heater winding, electrical power may be applied to produce a heating pattern similar to radiation. Comparison of the temperature rise due to electrical energy with the temperature rise caused by radiation energy E can thus yield the value of E. This comparison procedure approximates closely a null method, so that the actual temperature rise need not be known.

The electrical energy delivered to the absorbing element may be determined with great accuracy. The resistance (R) of the heater winding has a low temperature coefficient, and so may be measured accurately. The current (I) in the winding may be found by measuring the voltage across a precision resistance in series with the heating winding. The power delivered to the absorbing element is then just I^2R.

For the power to be considered as an absolute quantity, the voltage and resistance measurements must be traceable to Australian primary standards. A Hewlett-Packard 3457A Digital Multimeter was used as a transfer standard. It was calibrated against the ANSTO secondary standard 1K resistor and standard cell, both of which are calibrated every 2 years by the CSIRO, National Measurement Laboratory (NML) in Sydney.

The HP 3457A has itself been calibrated over the ranges 30 mV, 300 mV, 3 V, 30 V, and 300 V, with linearity determined over each range.

These electrical secondary standards provide the legal traceability required for the absolute determination of energy in the absorbed dose calorimeter.

2.4 Energy Response of Calorimeter

The total cross-section for absorption of bremsstrahlung in the microcalorimeter absorber comprises atomic and nuclear components. In the energy range 1 to 25 MeV, the predominant atomic processes are Compton scatter and pair production. Charged particles produced by these processes lose their energy by multiple collisions with atomic electrons; in graphite, all this energy is believed to appear as heat.

For photon energies above the (γ,n) threshold neutrons may also be produced. These neutrons also lose their energy by multiple scattering, having a diffusion length of approximately 40 cm in graphite. The nuclear cross-sections are very much less than those of the atomic processes.

Because no significant fraction of catastrophic effects occur (such as Wigner effect), all the incident photon energy is degraded to heat. For this reason, the temperature rise induced by absorption of bremsstrahlung is independent of the photon energy spectrum, i.e. the energy response of the calorimeter is flat.

This feature of "flat energy response" is of great value in establishing a primary standard of measurement for absorbed dose in the energy range 1 to 25 MeV. For all bremsstrahlung peak energies, the energy introduced by electrical means is thus assumed to produce the same temperature rise as the energy deposited by the radiation.

Thus the calorimeter provides an absolute standard of measurement over the energy range 1 to 25 MeV of interest here.

2.5 Configuration of the Urquhart Calorimeter

Details of the calorimeter design have been published previously by Urquhart et al [1978]. A non-scale diagram is given in Figure 1. The device comprises 4 nested graphite components, designated absorber, adiabatic jacket, mantle and phantom.

This configuration was determined by two fundamental constraints. Firstly, adiabatic heating of the absorber is required. The absorber is the detecting element; any heat losses from the absorber yield an error in the absorbed dose determination.

Secondly, temperature stability of a high order is required if the design temperature resolution of 15 μK is to be achieved.

To ensure adiabatic heating of the absorber, it is completely enclosed in an electrically heated adiabatic jacket. During radiation and electrical runs, the temperature differential between jacket and absorber is held constant, thus providing quasi-adiabatic operation.

Temperature stability is provided by two nested ovens enclosing the adiabatic jacket/absorber assembly. The inner oven is designated the "mantle", the outer oven the "phantom". Both are independently temperature controlled under software direction from a computer.

All 4 calorimeter components are thermally isolated from each other, being mounted on low thermal conductivity Delrin pins. The vacuum gaps between the components are designed to be 0.25 mm. The entire unit is mounted in a vacuum vessel, which is pumped down to a hard vacuum. In addition, the surfaces are aluminium plated to reduce radiation losses. The resulting heat transfer coefficients between adjacent components lead to a fortunate compromise in the need to eliminate temperature drifts while at the same time allowing a margin for temperature control.

In 1981, it became necessary to repair the calorimeter as a result of the failure of the thermistor in the absorber. The jacket was cut open and a new thermistor (FENWAL TYPE GC 32L10) embedded in the absorber. As a result of this work, Tables 2, 3 and 4 of report AAEC/E455 require revision. The revised tables are given in this report as Tables 1, 2 and 3.

The masses (in grams) of graphite in the absorber, jacket, mantle and phantom are 1.66983, 12.3347, 65.22854 and 2199.81204 respectively.

For a more complete description of the calorimeter construction, see Urquhart, Johnson and Badger [1978].

2.6 Quasi-adiabatic Operation

The process of adiabatic heating is said to occur when no heat is lost from the object in question. During irradiation of the absorber, heat may be lost by radiation (minimised by aluminium plating), convection (minimised by vacuum enclosure) or conduction (minimised by method of support). Also, heat may flow along the thermistor leads and heater wires.

By maintaining the absorber heat reservoir (the adiabatic jacket) at the same temperature as the absorber, these heat losses may be reduced to negligible proportions. For example, the thermistor leads and heater wires are wound inside the jacket, so that no temperature differential exists which would allow conduction to occur.

Adiabatic operation of the calorimeter is a requirement for equation (1) to yield the correct absorbed dose. In practice, this condition of strict adiabatic operation (no heat flow), cannot be met. The sensing thermistor embedded in the absorber is one arm of a sensitive Wheatstone bridge. Driven by a mercury battery, this thermistor dissipates approximately 1 μW. By contrast, an absorbed dose rate of .01 $Gy.s^{-1}$ which is representative of the output from the ANSTO El Dorado ^{60}Co unit, corresponds to a power absorption of 10 μW. Clearly, the thermistor self-heating is a significant fraction of the incident radiation heating.

Further, because the adiabatic jacket encloses the absorber completely, it acts as a heat reservoir. The absorber can only be at the same temperature as the jacket if no external power flows to the absorber. Consequently, the absorber will always be at a higher temperature than the jacket, as there is always a heat flow toward the jacket.

Provided the heat flow from the absorber is only that power generated in the thermistor, equation (1) may still be used. This form of operation is referred to in this text as QUASI-ADIABATIC.

In the operation of the calorimeter, provided that the temperature drift-rate of the absorber is the same before and after heating, the process is considered to be quasi-adiabatic. All the following irradiation and electrical heating control algorithms are designed to produce this condition of equal drift-rates.

2.7 Newtons Law of Cooling

Due to heat transfer between adjacent components of the calorimeter, any change (due to external power sources) affecting one component inevitably affects all the components. This interdependence could lead to difficulties in temperature control, especially with respect to adiabatic operation when the external power field (radiation beam) is not homogeneously applied.

However, the behaviour of this sytem is well described by Newtons Law of Cooling, which may be applied to each of the 4 components. The resulting 4 simultaneous first order differential equations can be used to develop the necessary temperature control algorithms. Indicating the absorber, jacket, mantle and phantom by the subscripts 1,2,3 and 4; and the temperature, heat capacity, heat transfer coefficients and power flow by T, C, K and P, with t the time, the equations are:

$$\frac{dT}{dt}^1 = -\frac{K}{C}_1^1 T_1 + \frac{K}{C}_1^1 T_2 + \frac{P}{C}_1^1 \tag{6}$$

$$\frac{dT}{dt}^2 = \frac{K}{C}_2^1 T_1 - \frac{(K_1+K_2)}{C_2} T_2 + \frac{K}{C}_2^2 T_3 + \frac{P}{C}_2^2 \tag{7}$$

$$\frac{dT}{dt}^3 = \frac{K}{C}_3^2 T_2 - \frac{(K_2+K_3)}{C_3} T_3 + \frac{K}{C}_3^3 T_4 + \frac{P}{C}_3^3 \tag{8}$$

$$\frac{dT}{dt}^4 = \frac{K}{C}_4^3 T_3 - \frac{(K_3+K_4)}{C_4} T_4 + \frac{P}{C}_4^4 \tag{9}$$

A procedure for solution of equations (6) - (9) is given by Zill [1982]. Briefly, equation (6) - (9) may be written as

$$\underset{\sim}{T}' = A\underset{\sim}{T} + \underset{\sim}{P} \tag{10}$$

where prime indicates differentiation with respect to time, A is a constant matrix and $\underset{\sim}{P}$ is time dependent. The solution of equation (10) depends on determination of the fundamental matrix, $\phi(t)$, of the equation

$$\underset{\sim}{T}' = A\underset{\sim}{T} \tag{11}$$

Equation (11) is the homogeneous case of equations (6) - (9), i.e. P_i is constant. This case has been solved previously by Domen and Lamperti [1974] for a 3-body calorimeter and by Sherlock [1987] for a 4-body calorimeter.

Consider a collection $\phi_1(t), \ldots, \phi_n(t)$ of solutions of the n-dimensional first-order linear homogeneous system given by equation (11). This collection is a fundamental system of solutions if it is linearly independent. The importance of a fundamental system of solutions of a linear system is that we may describe any solution of the system in terms of the fundamental system of solutions, i.e. we need only properties of the fundamental system in order to determine the behaviour of any solution.

Then any solution $\phi_j(t)$ may be written

$$\phi_j(t) = [\phi_{ij}(t), \ldots, \phi_{nj}(t)] \tag{12}$$

and $\phi(t)$ forms a fundamental matrix whose columns form a fundamental system of solutions of (11). Note that the determinant $|\phi(t)|$ is called the Wronksian of ϕ.

Solution of equation (10) takes the form

$$\underset{\sim}{T}(t) = \phi(t)\ \underset{\sim}{T}(0) + \int_0^t \phi(t-s)\ \underset{\sim}{P}(s)\ ds \tag{13}$$

where $\underset{\sim}{T}(0)$ is the temperature vector at time zero. However, the boundary conditions at time zero require that the integral term vanish and $\phi(t)$ equal the identify matrix, i.e.

$$\lim_{t \to 0} \phi(t) = I \tag{14}$$

The fundamental matrix $\Omega(t)$ satisfying these boundary conditions is given by

$$\Omega(t) = \phi(t)\ \phi^{-1}(0) \tag{15}$$

yielding the general solution

$$\underset{\sim}{T}(t) = \Omega(t)\ \underset{\sim}{T}(0) + \int_0^t \Omega(t-s)\ \underset{\sim}{P}(s)\ ds \tag{16}$$

Equation (16) is a completely general solution to equation (10), i.e. power is a continuous function of time. This solution is appropriate to the use of analog controllers for temperature control of the calorimeter.

In practice, the digital system used varies the power in discrete steps, with a duty cycle of order 10 seconds. Thus the system may also be followed using the homogeneous case with new solutions computed every duty cycle. This yields a simplified set of solutions

$$T_i(t) = \sum_{j=1}^{4} \beta_{ij} e^{-r_j t} + T_i(\infty) \qquad (17)$$

with the terms given by Sherlock [1987].

Equation (17) forms the basis of a calorimeter computer simulation program which may be used to evaluate systematic errors in the quasi-adiabatic operating procedure.

3. CONFIGURATION OF CALORIMETER CONTROL APPARATUS

3.1 System Structure

The upgraded electronics provided for the Urquhart graphite micro-calorimeter were required to meet a number of criteria. The most important of these was the desirability of using computer software to provide monitoring and control of the device. This approach facilitates optimisation of signal processing and the rapid development of sophisticated control algorithms.

A second criterion was that the computer and instruments should be able to communicate with each other as an "off-the-shelf" feature, since time and finances did not permit the construction of special purpose interfaces. For this reason, the IEEE-488/1978 interface bus was specified for all instruments and the controller (ANSI/IEEE-488-1978).

The initial rebuild required that continued use be made of the existing Keithley 147 analog nanovoltmeters. This system is shown in block diagram (Fig.2); the system was used to perform standardisations under the ANSTO AECL El Dorado 6 Cobalt-60 unit and the Varian Clinac 1800 linear accelerator installed at Royal North Shore Hospital, Sydney.

With financial support from the Department of Oncology, Westmead Hospital, two Keithley 181 digital nanovoltmeters were used to replace the Keithley 147 units. The block diagram for the improved system in given in Fig.3; this system was used to perform standardisations under the Philips SL25 linear accelerator installed at Westmead Hospital.

Operation of the system may be explained with reference to Figure 2, which is a block diagram of the electronic and electrical components. The IEEE-488 bi-directional data bus is indicated by double-ended arrows, while single-ended arrows indicate data flow on the bus in one direction only.

The object of the system design is that all operations, including temperature control and monitoring, be under software control.

Consider first the thermistors. The phantom thermistor bridge output goes directly to the HP 3457 DMM. This voltmeter has adequate resolution for "coarse" control of the phantom temperature. The computer responds to the signal from the HP 3457 by providing a control signal to the Topward TPS 4000 power supply via the HP 3497 voltage digital-to-analog converter (VDAC) plug-in card. The output of the TPS 4000 then goes directly to the

phantom 114Ω control heater. Resolution of the phantom temperature control is approximately 100 μK, as determined by the control power fluctuations drawn from the TPS 4000.

The mantle thermistor operates in a similar fashion to the phantom. However, in this instance high-resolution temperature monitoring is required, comparable to that for the absorber. Accordingly, the bridge output goes to a Keithley 147 nanovoltmeter (or in Figure 3, to a Keithley 181). The Keithley 147 nanovoltmeter has an analog output; this output is connected to the HP 3478 DMM via a relay multiplexer card in the HP 3497 data acquisition unit (DAQ). The computer responds to the signal from the HP 3478 by controlling the current digital-to-analog converters (IDAC's) in the HP 3497 DAQ. These latter IDAC's provide power directly to the 108Ω and 87Ω heaters in the mantle. Details of the control process are given in Section 5 of this report.

The absorber thermistor is monitored by the computer in the same manner as for the mantle thermistor. However, no control functions are generated from the absorber thermistor signal.

The "calibrator", which provides electrical power to the absorber and adiabatic jacket during electrical heating, is also operated by the computer. The relay (shown in Figure 7 as numbered contacts), receives a control voltage from the VDAC in the DAQ. A third IDAC in the DAQ acts as a current source for the calibrator, which normally sinks this current in two ballast resistors, of 6190Ω and 778Ω respectively. During electrical heating, the relay contacts change, redirecting the IDAC current to the 776.6Ω absorber heater and 6168Ω heater in the adiabatic jacket.

In addition, the voltages across the 770.058Ω standardised resistor and across the absorber heater winding (776.6Ω) are directed via the calibrator and multiplexer card to the HP 3478 DMM. This latter instrument has been calibrated against the HP 3457 secondary standard DMM.

Finally, the computer is provided with the means to operate the radiation source. Both a Varian Clinac 1800 and El Dorado 6 Cobalt teletherapy unit are shown in Figure 2, as alternatives. The HP 3457 DMM has an added feature in the form of a plug-in multiplexer card which includes two actuators. This feature enables the computer to terminate a Clinac 1800 exposure by breaking the door interlock circuit. In the case of the El Dorado 6, the exposure may be both commenced and terminated by a logical current pulse from the fourth IDAC in the DAQ.

The operations implied in Figure 3 are similar; however, the need for multiplexing the nanovoltmeter outputs is eliminated as the Keithley 181 nanovoltmeters are provided with IEEE 488 interfaces.

3.2 Specification of System Components

In the temperature monitoring circuits, the critical specification affecting resolution is the input noise level of the voltmeter used. In Table 4, the characteristics of the system voltmeters are summarised.

The output noise characteristics of the Keithley models 147 and 181 are of the order of the Johnson noise from the absorber Wheatstone bridge. However, no figure is given for the Hewlett Packard DMM's. The resolution claimed for the HP 3457 is 10 nV. This is highly misleading, as in fact the noise level of this instrument connected to the absorber bridge is greater than 1 μV. It should be noted that the Keithley instruments are optimised for nanovolt measurements. While the HP instruments must average many readings to obtain resolution below 1 μV, the Keithley 181 makes measurements down to 10 nV with 30 nV noise in a single conversion.

For these reasons, the Keithley instruments are applied to reading the bridges while the HP instruments are suitable for determining the power level flowing from the calibrator during electrical heating.

When using the Keithley 147's, it is necessary to multiplex their analog outputs into the HP 3478. The multiplexer card was an HP 44421A supported on IEEE-488 bus by the HP 3497A Data Acquisition Unit. Each of the 20 channels on this card consist of three reed relays, one each for High, Low and Guard lines. These relays feature low thermal offset characteristics. In operation on the calorimeter, there was no evidence of noise or thermal offsets arising from the use of this multiplexer.

The HP 3497A also features dual voltage and current digital to analog converters (VDAC and IDAC). Specifications for these devices are summarised in Table 5. One IDAC card was used as a power supply for the mantle heaters, while one channel of a second IDAC card provided power to the calibrator circuit. One channel of the VDAC card was used as a controller for the Topward TPS 4000 dual power supply. The Topward provided current to the phantom heater. A test of this arrangement showed that the stability of the Topward was 1 μV at the programmed value, which was quite remarkable.

A compilation of the system components is given in Table 6.

3.3 Vacuum System

Of conventional design, the vacuum system comprises a backing pump, oil diffusion pump and gauges. The specification is for an environmentally non-polluting system which can achieve 10^{-6} Pa at the gauge head.

An Edwards EDMZ series 04634 direct-drive backing pump provided quiet, reliable backing pressure to the Edwards series EO2 oil vapour diffusion pump. Chilled water from a Leybold-Heraeus closed circuit chiller unit provided cooling for the diff pump. Long hoses enabled the chiller unit to be remote, so that no heat was dissipated in the vicinity of the calorimeter. In combination with an oil-mist eliminator on the backing pump outlet, these features of quiet, cool operation allowed the calorimeter to be operated in a treatment room while the room was in clinical use.

Vacuum connection to the calorimeter was via a 1m long flexible stainless steel coupling hose. Some vibration from the rubber-mounted backing pump was transmitted to the calorimeter vacuum vessel via this hose.

No cold trap was used above the diff pump. There exists the possibility of a small amount of oil backstreaming into the calorimeter over a period of time.

Other than a corrosion problem in the water chiller thermostat sensor pipe, the vacuum system met the design requirements, performing reliably over some 5000 hours of service.

4. TEMPERATURE MONITORING

4.1 Thermistor Bridges

Calorimeter temperature measurements are made using a single thermistor as one arm of a Wheatstone bridge. The thermistor arm of the bridge is connected to the rest of the bridge by a 10 m twin core, double-shielded, low thermal cable supplied by Leeds and Northrop. Thus the bridges can be operated in the control room adjacent to the irradiation facility.

Claims have been made [DuSautoy, 1985] that DC bridges used in this application are noisy due to thermal e.m.f's. No such difficulties have been experienced at ANSTO. Occasional periods of noisy operation have been observed on the absorber bridge. This noise corresponds to an intermittent breakdown in the electrical insulation of the thermistor leads inside the calorimeter. The problem seems to arise at initial pump-down, disappearing after a stable vacuum is in place. This failure mode is a cause for concern and may limit the useful life of the calorimeter.

A second source of noise concerns the mercury batteries (Mallory Duracell TR133R 4.05V) used to drive the thermistor. When the cells are discharged below 4V, they may become noisy. As this corresponds to 3 months usage, the batteries are simply replaced at that time.

Circuits for the bridges are given in Figures 4, 5 and 6.

4.2 Impedance Match of Bridge to Nanovoltmeter

The output impedance of the bridges is essentially determined by the thermistor resistance. Application of Thevenins theorem gave a value of the order of 2300 Ω when the absorber and mantle bridges are at operating temperature (28°C). Since the input impedance of the Keithley 147 is greater than 1 MΩ, and that for the Keithley 181 greater than 1000 MΩ, no difficulties were experienced with voltage division by the nanovoltmeters.

4.3 Unbalanced Operation of Bridge

In conventional operation, a Wheatstone bridge is used as a null device, i.e. it is run in a balanced condition so that the output voltage is zero. This avoids the non-linear characteristic of the bridge output voltage, but implies that a variable resistance be placed in one arm of the bridge to allow for manual setting of balance.

This manual operation is inconvenient in a computer controlled apparatus which is designed to run unattended. A simple solution is to allow the bridges to run off-balance, having first chosen the balance condition.

In the ANSTO device, both the phantom and mantle bridges are completely fixed. At balance condition, the phantom runs at 27.5°C and the mantle at 28°C. When the absorber is in equilibrium with the mantle, the latters balance resistor (Leeds and Northrop Decade Resistor) is adjusted to give a zero voltage output. No further adjustments are made to the absorber bridge operating point.

Off-balance operation of the absorber bridge is acceptable because the output voltage swing is very small, only 5 μV compared to an input voltage of 4.05 V. With such a small swing, the range of operation is essentially linear.

Over 5 consecutive runs the voltage swing may be 30 μV. However, the data are collected in matched pairs, one electrical run followed by one radiation run, so that the voltage swing over each pair remains small.

After 5 runs (of 10 Gy each), the absorber is allowed to cool to its original setting. This corresponds in practise to one working days' operation.

The correction factor for unbalanced operation is given in a succeeding report.

4.4 Circuit Shielding

Successful measurements at very low voltages (μV) require particular care related to shielding, thermo-electric effects, ground loops, magnetic fields and Johnson noise.

By far the most important of these effects is electrostatic shielding. All signal conductors must be enclosed in a correctly configured Faraday cage. No break in the cage is permissible.

Design rules for shielding have been given by Morrison [1977]. They are restated here and their application to the calorimeter discussed.

There are two rules; the first of these is:

'An electrostatic shield enclosure, to be effective, should be connected to the zero signal reference potential of any circuitry contained within the shield'.

This rule requires that the shield must be tied to zero-signal reference potential. If the signal is earthed or grounded, the shield becomes earthed or grounded. Earthing or grounding the shield makes no sense if the signal is not earthed or grounded.

The second rule is:

'The shield conductor should be connected to the zero-signal reference potential at the signal-earth connection.'

This procedure ensures that parasitic currents will flow in the shield only and not in the signal conductors. The shield can be thought of as a drain path to carry unwanted current back to an earth point. Further, the rule can only be applied when 2-conductor shielded wire is used. Single shielded wire (co-ax) obviously requires that the shield and zero-signal reference conductor be one and the same. Since unwanted current can only flow in the shield, pick-up cannot easily be controlled with this type of cable.

These rules were applied using the following technique

4.4.1 Cable Harness

The 10m cable harness connecting the calorimeter to the bridges, calibrator and heater power supplies were made with Leeds and Northrop supplied dual core, double shielded, low noise, low thermal cable. Cable terminations were made using Amphenol BNC dual pin shielded connectors, types 554-86/473 (plug) and 554-85/280 (socket).

4.4.2 Absorber Bridge

The Leeds and Northrop type 4750 decade resitance box is fully R.F. shielded. Accordingly, it was modified, with the absorber bridge being built directly inside the box. The external binding posts were disconnected and the holes R.F. shielded. Amphenol BNC

shielded connectors were mounted on the front panel to allow connection of the absorber thermistor and bridge output. The bridge batteries were solder-connected with no switch.

4.4.3 Mantle and Phantom Bridges

These bridges were built into a common cast-aluminium box, again using shielded dual pin sockets and no switches.

4.4.4 Calorimeter

The spun aluminium Faraday shields enclosing the calorimeter were correctly wired into the shielding circuit. A bank of 10 BNC sockets were mounted on a panel that formed part of the screening. A break in the shielding was necessary where the vacuum hose entered the Faraday shield. The vacuum hose was electrically isolated from the vacuum system by a machined Delrin fitting.

4.4.5 Instrument Connections

Whenever possible, the shielding design rules were applied to the instrument connections. However, the instrument designs left something to be desired. For example, the input to the Keithley 147 nanovoltmeter is a shielded, dual pin, low thermal socket. However, the shielding ends right there at the panel, and does not go through to the shield surrounding the input valves. As a compromise, the front panel shielding was jumpered to the rear panel output screen. In the event, no problems were encountered with this termination.

Instrument low and ground were connected at the HP 3478 DMM. It should be noted that the bridges are fully floating, except at the single grounding point. Tests with the ground disconnected showed no difference to the case when the ground was connected. Evidently connecting low to shield was adequate in this application.

4.5 Thermal EMF's

Spurious voltages and currents may be a problem in low-voltage measurements as a result of thermal effects; in particular Seebeck, Peltier and Thomson effects require consideration.

4.5.1 Seebeck Effect

If a circuit is formed of 2 dissimilar metals, an EMF depending on the temperature difference of the junctions is developed. For wires

with thermoelectric power η in a temperature gradient ∇T, the EMF developed is given by

$$EMF = \int_{loop} \eta \, \nabla T \, dx \qquad (18)$$

It is generally considered that the EMF is formed at the junction, with the temperature gradient along the wires unimportant.

However, it is clear from (18) that the Seebeck effect is a bulk property of the circuit. Indeed, an EMF cannot be generated at the junction. To avoid Seebeck effect, junctions should be made with similar metals; leads must be identical with respect to thermoelectric power; and the paths of the wires should be identical.

With respect to the calorimeter cable harness, the latter two conditions are met by the type of cable used.

In the case of the junctions, common practices are to clamp bare copper leads together on a thermal reservoir to avoid introducing dissimilar metals; to use low thermal cadmium-tin solder; or to use crimped cold-welded copper-to-copper junctions. However, these practices focus on the junction, rather than on the bulk effect indicated by equation (18). In fact, these methods may cause more problems than they solve. For example, copper-to-copper clamping may, due to oxidation, produce copper to copper oxide connections which have thermoelectric potentials of 1000 $\mu V.K^{-1}$. Further, cadmium-tin solder is very difficult to apply and after a period of time the junctions may go open circuit.

Accordingly, all connections used outside the calorimeter were either conventionally soft-soldered or in the case of BNC connectors, silver to silver interference fit. Internal calorimeter connections were either welded or crimped.

Prior to rebuild of the calorimeter electronics, the absorber and mantle bridges were enclosed in temperature controlled ovens, with the intention of eliminating thermal effects. This approach was reviewed and considered both unnecessarily complex and in excess of requirements. Accordingly, the re-built bridges were housed in 10cm

wall thickness styrofoam boxes, with no temperature control mechanism.

In practice, no problems traceable to Seebeck effect were experienced.

4.5.2 Peltier and Thomson Effects

Peltier in 1834 found that when a current flows across the junction of two metals it gives rise to absorption or liberation of heat, dependent on direction of current flow. Thomson found that when a current flows along a copper wire whose temperature varies from point to point, heat is liberated at any point P where the current at P flows in the direction of the flow of heat.

In the present application, the currents involved are very low, and no account is taken of these effects.

4.6 Ultimate Noise Limitations

Johnson noise has been previously discussed in Section 2.2. of this report. The inherent white noise level of the absorber bridge is at least 30 nV in a single reading. This noise is dependent on the instrument bandwidth, so nothing can be done to reduce the noise in a single reading.

However, an actual calorimeter temperature rise determination is comprised of many readings accrued over drift and heating periods. Typically, the drift periods are 600s, and the heating period 200s, with temperature readings taken every 10s, ie. some 140 readings.

During analysis, straight lines are fitted to these data and the temperature rise determined from their intercepts. These sets of data are replicated at least 10 times, so that a standard deviation may be computed for the temperature rise.

Assuming systematic effects due to drifts have been eliminated, the standard error thus obtained is considered to represent the total noise of the system.

4.7 Thermal Response Time

Temperature gradients occur inevitably as a result of non-uniform application of power to the graphite elements comprising the calorimeter. Accordingly, the response of the temperature sensing thermistor may depend on its position in a calorimeter element.

The worst case applies to electrical heating of the absorber element. In an effort to provide uniform heating, the absorber heater winding is composed of a spiral winding in 2 planes, with the thermistor imbedded in the centre of the rear plane. Correct operation of this assembly requires rapid heat transfer from the heater wire and throughout the graphite. An alternative arrangement is to use a thermistor placed at a single point in the absorber.

Work by Huntley [1985] indicates that heat transfer in graphite is very rapid, with temperature uniformity achieved in a few seconds. For example, with single thermistor heating at a power level of 23 μW, the temperature gradient from centre to edge of the absorber is only 1% (100 μK). Electro-graphite, type EY927 used in the calorimeter, has a thermal conductivity of approximately 150 $W.m.^{-1}K^{-1}$ (Urquhart et al, 1978).

In the case of the Urquhart calorimeter, there is no evidence of thermal lag in heating the absorber. However, the mantle thermistor does show non-linear effects at the start and finish of heating; this effect is almost certainly due to positioning of the thermistor with respect to the heater winding. Again, the response time for this effect is of the order of 2 seconds, providing further evidence of the rapid heat transfer in graphite.

A second indicator of thermal response time concerns operation of the temperature controllers. Any significant lag in thermistor reading would give rise to oscillations in the control power. No such oscillations occur. For all practical purposes, the thermal response of the absorber thermistor may be considered instantaneous.

4.8 Storage of Data

During either a radiation or electrical calibration run, the computer is fully occupied maintaining temperature control and monitoring temperature. Data analysis must be performed off-line at a later time; for this reason, data is stored in read-write memory during a run, then stored on a floppy disc at the end of the run.

During every duty cycle, the temperature and time since start of run is stored for each of the absorber, mantle and phantom. Also for every duty cycle in an electrical calibration, the voltages across the standardised resistor (in the calibrator) and the absorber heater are also stored.

5. CONTROL OF TEMPERATURE - STEADY STATE

5.1 Temperature Control Theory

The design considerations given in Sections 3 and 4 of this report are aimed at producing a stable and repeatable behaviour in the temperature performance of the calorimeter. With spurious effects eliminated, the response of the calorimeter is well described by Newtons Law of Cooling, given in equations (6) - (9).

It remains to place the calorimeter in a steady state condition ($\frac{dTi}{dt} = 0$) at above ambient temperature. The phantom is typically run at 27.5°C, with the mantle at 28°C prior to experimental work. Due to self heating by the absorber thermistor, both the absorber and jacket will run slightly warmer than 28°C. Since the components all interact to some degree, a control system is required which can maintain a steady state.

The behaviour of governors, as given by Maxwell [1868], indicates the nature of the control problem:

'It will be seen that the motion of a machine with its governor consists in general of a uniform motion, combined with a disturbance which may be expressed as the sum of several component motions. These components may be of 4 different kinds:

1. The disturbance may continually increase.
2. It may continually diminish.
3. It may be an oscillation of continually increasing amplitude.
4. It may be an oscillation of continually decreasing amplitude.

The first and third cases are evidently inconsistent with the stability of motion; and the second and fourth alone are admissible in a good governor'.

Solutions of equation (17) do not admit of oscillatory temperature behaviour in the calorimeter. Rather, such oscillations must be produced by the controller. Such oscillations are described by Ivanoff [1934], in the application of "floating" and "proportional" controllers.

In the case of the Urquhart calorimeter, independent controllers act on the mantle and phantom; by their action, the temperatures of the jacket and absorber remain constant.

5.2 Proportional Control

Define the temperature "set-point" T_S as the desired temperature to be maintained by a controller, e.g. 27.5°C for the phantom. If at any instant the temperature is too low, power must be applied to the body; if too high, power must be lost. As the system is designed to run above ambient temperature, only heating is necessary for control.

In a "proportional" controller, the power applied is made a function of the difference between the set-point and instantaneous temperature. Such a controller provides a steady approach to the set-point, with no overshoot. With G_P the gain, the proportional controller algorithm for the mantle may be written, using the symbols of equations (6) to (9), as:

$$P_3 = K_3 G_P (T_S - T_3) \tag{19}$$

Substituting equation (19) in equation (8) yields

$$T_3 = \frac{K_2 T_2 + K_3 T_4 + K_3 G_P T_S}{K_2 + K_3 + K_3 G_P} \tag{20}$$

The inference from equation (20) is that T_3 can only equal T_S for infinite gain! i.e. a proportional controller can never drive T_3 to the set-point.

This behaviour can be understood by realising that P_3 reduces as T_3 approaches T_S, to a point where the power loss from the mantle to the phantom matches the power input to the mantle, i.e.

$$P_3 = K_3 (T_3 - T_4) \tag{21}$$

Failure in this manner to reach the set-point can lead to drifts, as T_3 is then influenced by T_4. A similar problem then besets the phantom controller, as T_4 can be influenced by the ambient temperature represented by the vacuum vessel. Recall that room temperature variations are of the order of 1°C, while stability is required at 5 orders of magnitude less than this. As high gain values can lead to instability in the instrument when operated with a fixed duty cycle, an improved algorithm based on the proportional controller is desirable.

5.3 Integral Controller

With the proportional controller algorithm of equation (19), there is always present an error term δ such that

$$\delta = T_s - T_3 \tag{22}$$

Consider the controller operates with a fixed duty cycle, i.e. the power flow is adjusted every 10 s, according to the temperature which is also determined once each cycle. Then an additional power term is required such that

$$_nP_3 = K_3 G_P \delta_n + K_3 G_I \sum_{i=1}^{n} \delta_i \tag{23}$$

where $_nP_3$ is the power applied in the n th duty cycle; first term is the proportional controller of equation (19); the second the integral control term, with gain G_I.

This algorithm works remarkably well on the calorimeter. The set-point temperature is rapidly approached and then maintained. When δ_i is large, i.e. requiring many control cycles to reach T_s, then the integral term builds up and produces an overshoot. With a conservative choice of G_I, the oscillations introduced by the integral term damp rapidly.

5.4 Differential Controller

The controller given by equation (23) is adequate for most work on the calorimeter. However, on start-up from cold the integral term can become excessive, causing too large an offshoot. During this period, the integral term may be set to zero.

An alternative is to add another term, which varies with the rate of change of δ_i. With G_D the gain of the differential term, the controller algorithm, equation (23), becomes

$$_nP_3 = K_3 G_P \delta_n + K_3 G_I \sum_{i=1}^{n} \delta_i + K_3 G_D (\delta_i - \delta_{i-1}) \tag{24}$$

In practice, the differential term is only useful starting from cold. At steady state, the differential term is dominated by noise and is ineffective. The integral term is sufficient to drive T_3 within the noise band around T_s.

5.5 PID Controller

The controller algorithm given by equation (24) is referred to as a proportional-integral-differential or PID device.

Optimum performance of the PID depends on the choice made for the gains G_P, G_I and G_D. In the case of the calorimeter, the gains were determined by trial and error.

5.6 Heater Windings

The massive phantom (2200g) is provided with a 114Ω heater winding driven by a Topward TPS 4000 power supply. In the steady state, the current drawn by this heater is approximately 50 mA, giving a 5°C temperature differential between the calorimeter and ambient. During startup, when rapid heating is required, a maximum current of 150 mA brings the phantom to 27.5°C in 30 minutes. The heater winding is protected by zener diodes which limit the power supply voltage to a maximum of 17V.

The mantle is provided with two heaters, of resistances 108Ω and 87Ω. Temperature differential between the phantom and mantle of 0.5°C is set by placing a fixed current into the 108Ω winding. Balance of power required for temperature control and adiabatic operation is provided by the 87Ω heater. This stragegy yields very high power resolution for the 87Ω heater. Both mantle heaters are protected from inadvertent overload by zener diodes.

All active heaters are controlled by the PID algorithm implemented by software in the HP 86 computer.

6. CONTROL OF TEMPERATURE DURING IRRADIATION

6.1 Initial Drift

Prior to irradiation, a period of 600s is allowed during which temperature data are collected. Analysis of the 'drift period' can then establish the stability and noise level of the absorber temperature.

Control during this period is via the PID algorithm applied to mantle and phantom, the controllers acting independently.

6.2 Irradiation Period

The control process during irradiation (typically for 200s) is drastically modified compared to the initial drift. The radiation penetrates all components of the calorimeter, which respond instantaneously to the power flow in the beam.

With the chief function of the phantom being to isolate the calorimeter internal components from the environment, the phantom is run at constant temperature. To maintain this condition during irradiation, the power supplied to the phantom electrically must be reduced by the amount of power absorbed from the radiation beam.

Indicating the dose rate by D_r ($Gy.s^{-1}$) and the mass of the phantom by M_4, then the power incident on the phantom is given by

$$P_P = D_r \, M_4 \, F_p \tag{25}$$

There is a considerable dose gradient both longitudinally and laterally in the phantom; indeed, some parts of the phantom receive only scattered radiation. To account for this, the factor F_p corrects the mass of the phantom to that effective mass corresponding to total uniform radiation. This quantity was determined experimentally to be 0.4 for 6 MV bremsstrahlung.

With the electrical power P_e prior to irradiation, then the reduced electrical power P_k is just

$$P_k = P_e - P_p \tag{26}$$

The corresponding reduced current I_k (mA) is then

$$I_k = 1000 \left\{ \left(\frac{I_e}{1000}\right)^2 - D_r \frac{M_4}{114} \cdot F_p \right\}^{\frac{1}{2}} \qquad (27)$$

The phantom power supply is then programmed to deliver I_k at the moment of irradiation.

Given the requirement for adiabatic operation, the situation with respect to the mantle is considerably more complex. In the first instance, the adiabatic jacket, being heated fairly evenly by the beam, provides for reduced heat loss from the absorber.

However, this passive behaviour of the jacket is not adequate for true quasi-adiabatic operation. Not all the mantle is in the beam, so that heat will be lost from the jacket, with consequent losses from the absorber. During a 200s exposure, these losses may be significant, particularly toward the end of the run when the jacket-to-mantle temperature differential is approaching its maximum value.

True quasi-adiabatic operation thus requires that the mantle also rise in temperature at the same rate as the absorber and jacket. This requirement is quite different from the temperature control process required during the drift period.

Initially, an attempt was made to use the temperature of the absorber as a parameter for active control of the mantle. However, this and other approaches using active control could not be made to work. The difficulty is that the temperature of each component depends on the previous history of power application, resulting in an arbitrary phase relationship at any given time.

In view of the excellent temperature stability achieved by the calorimeter, it was realised that active control was not really necessary. Indeed, active control of the mantle was abandoned altogether in favour of computing the power requirements of the mantle from Newtons Law of Cooling. This approach proved to be highly successful.

Firstly, the heat transfer coefficient from mantle to phantom (K_3) was determined by experiment. In the steady state, $dT_3/dt = 0$ and $T_2 = T_3$. Taken from equation (8)

$$K_3 = P_3/(T_3 - T_4) \quad (28)$$

With the 108Ω heater drawing 10.5 mA, the 87Ω winding 4.1 mA and a temperature differential of 0.5°, the value found for K_3 was .0267 $W.K^{-1}$.

Then for an increase ΔT_3 in the temperature of the mantle, an additional amount of power $K_3 \Delta T_3$ was supplied electrically to the mantle. This power was added to that electrical power required for joule heating at dose rate D_r, determined with a correction factor of .13 for the mass of mantle not in the beam.

The above considerations lead to linear heating of the mantle, with the final drift rate of the absorber being very close to the initial drift rate. The requirement for quasi-adiabatic operation was then considered to have been met.

6.3 Final Drift

At the end of the irradiation, it was necessary to allow the mantle thermistor to equilibrate for 60s before taking the mantle temperature as the new set-point. The PID controller was then reactivated.

The phantom power was restored to its initial value at the instant of beam termination, the PID reactivated, and allowed to adjust to the new power flow from the now warmer mantle.

Final drift period was again 600s. A further period of 40 minutes was then allowed for equilibration prior to performing the next electrical heating cycle. In this fashion, repeat runs could be performed on an hourly basis.

7. CONTROL DURING ELECTRICAL CALIBRATION

7.1 Calibrator Circuit

Electrical heating of the absorber is performed in a manner designed to mimic the radiation heating profile. With the similar heating rates thus provided, departures from adiabatic operation are further minimised.

The calibrator circuit is designed to provide an amount of power to the absorber known absolutely. In this case, measurements of voltage and resistance traceable to Australian primary standards are required.

Contained in series with the IDAC power supply is a Leeds and Northrop manganin-wound low-temperature coefficient resistor. The resistor has a value determined by the National Measurement Laboratory (NML) of 770.058 ohms at 20.0°C. Voltage drop across this resistor is measured with an HP 3457A transfer standard DMM, also with a calibration traceable to NML. The same DMM also measures the voltage drop across the absorber heater resistance of value 776.6 ohms. In this manner the electrical power delivered to the absorber is known absolutely.

The calibrator circuit, given in Figure 7, includes ballast resistors so that the IDAC power supply sees a constant load, and is hence stable.

The calibrator is provided with a computer-operated, dry-contact, double-pole, changeover relay which selects either ballast mode or heating. The voltages across the standard resistor and absorber heater are monitored every duty cycle during an electrical calibration run.

Current to the adiabatic jacket is shunted by a 200 kΩ variable resistance. Adjustment of this potentiometer ensures that the temperature rises in jacket and absorber are made equal.

7.2 Intitial Drift Period

Control during initial drift is identical with Section 6.1.

7.3 Electrical Heating Period

Control during electrical heating is similar to Section 6.2, with simplifications due to the absence of radiation, i.e. there is no need to correct the phantom current at start of heating.

Also, all the power for heating the mantle is electrical, so that the correction factor for material not heated directly is unity. Again, the power supplied to the mantle is computed, with no attempt at active control.

7.4 Final Drift

Control during final drift is similar to Section 6.3. At the end of the run, the voltages measured from the calibrator are stored on flexible disc, along with the temperature and time data.

8. PERFORMANCE UNDER CONSTANT DOSE-RATE IRRADIATION

8.1 Implication of Quasi-Adiabatic Operation

Quasi-adiabatic operation has been discussed earlier in Section 2.6 of this report. The criterion provided there for quasi-adiabatic operation was that the absorber drift rates before and after heating be the same. A corollary to this requirement is that the temperature rise during constant power heating be linear.

Consider the results obtained during the standardisation of 6 and 18 MV bremsstrahlung beams from a Varian Clinac 1800 medical linear accelerator. The Clinac 1800 has an exceptionally accurate dosimetry system which both terminates treatment and provides a dose-rate servo control signal. Thus the dose-rate from this machine is particularly constant, quite comparable with a cobalt-60 teletherapy unit.

Drift rates and heating rates are given in Tables 7 and 8 for 6 and 18 MV respectively. For 6 MV, the mean percentage change in drift rate for radiation heating was found to be -.28 ±.57; for electrical heating, it was +.27 ±.43. Similarly for 18 MV, for radiation heating it was found to be .002 ±.08; for electrical heating it was -.12 ±.07. The confidence limit given is one standard deviation calculated from the replicate runs in Tables 7 and 8.

From these figures and Tables 7 and 8 it is apparent that the change in drift rate is very low; indeed, comparable to the random error involved in determining the drift-rate difference.

The linearity of heating and the noise level associated with the temperature readings may be assessed by an inspection of Figures 8 and 9. Straight lines have been fitted to the drift and heating periods. The linearity is good and the noise level low.

8.2 Errors in Absorber Heating

The absorbed dose rate in graphite was determined for each of the experimental runs given in Tables 7 and 8. The results are given in Table 9. The experimental runs were commenced at hourly intervals, each radiation run being followed by an electrical run. Equilibration between runs was rapid, as indicated by the constancy of the drift rate after five consecutive sets of runs (one days work).

The standard deviation of the mean for 6 MV was .15%, and for 18 MV .09%. These are gross errors, including all random error components from the calorimeter and the dosimetry system in the linear accelerator.

8.3 Mantle Bridge Characteristics

Response of the mantle thermistor during electrical and radiation heating is indicated in Figure 10 for 6 MV bremsstrahlung and in Figure 11 for 18 MV bremsstrahlung.

This response appears to be independent of beam energy. However, the anomalous behaviour at the start and finish of heating does depend on the amount of electrical power provided. During heating by radiation, a small amount of electrical power must be supplied to the mantle as not all the mantle lies within the beam. The anomalous behaviour of the thermistor is then much less than when full electrical power is supplied, which is the case in an electrical run.

At the end of the heating period, a delay of 60s is provided before selecting the mantle set-point temperature and restarting the PID controller. During this 60s period, the anomalous behaviour of the thermistor decays to a steady state value.

The anomaly appears to be related to the proximity of the thermistor to the heater winding. Apart from this odd behaviour, the mantle heating is otherwise linear, indicating the correct compensation has been provided for heat losses from the mantle to the phantom.

The data plotted in Figures 10 and 11 were obtained during run #1 of Tables 7 and 8.

8.4 Phantom Bridge Characteristics

Response of the phantom thermistor during electrical and radiation heating is indicated in Figure 10 for 6 MV bremsstrahlung and in Figure 11 for 18 MV bremsstrahlung.

The noise level was fairly high atthe time of the 18 MV runs. It should be noted that for these runs a DMM was used to monitor the phantom bridge

output, as no nanovoltmeter was available at that time. The configuration of the DMM input did not provide for full screening of the signal lines. Despite this, temperature resolution of this bridge was still of the order of 100 μK.

During the electrical runs, the phantom PID is in continuous operation and no temperature variations are observable. However, during radiation runs the electrical power supplied to the phantom must be reduced to match the input power from the beam.

The beam transients and controller response are visible in Figure 10, although rather dominated by noise in Figure 11. The scales in these figures are the same, and have been chosen to show that the transients are within an order or magnitude of the noise. With no power compensation at beam on, the phantom temperature would rise off the scale limits of these figures within 10s.

Temperature compensation of the phantom is considered effective, so that T_4 is considered constant at all phases of calorimeter operation.

9. CONCLUSION

The Urquhart graphite micro-calorimeter has been placed under computer control and used for the determination of absorbed dose under high energy photon beams.

In this report, control and monitoring techniques have been described, with an assessment of the performance achieved being given for 6 and 18 MV bremsstrahlung beams. Random errors have been reduced to near negligible proportions, while systematic errors have been minimised by achieving true quasi-adiabatic operation.

10. ACKNOWLEDGEMENTS

This program of measurement has been generously supported by Professor A.O. Langlands and Mr J. F. Drew, of Westmead Hospital; Dr R. Malik of Royal North Shore Hospital; Mr P. Cardew, of the Mater Misericordiae Hospital at Waratah; and Dr A. J. Leslie, of the Australian Institute of Health.

In particular, the author would like to pay tribute to the designer of the calorimeter, Mr D. F. Urquhart (retired), in view of the excellent performance of the device.

11. REFERENCES

1. OIML, 1988: International document: Secondary Standard Dosimetry Laboratories for the calibration of dosimeters used in radiotherapy. OIML Reporting secretariat SP-6-Sr 2: Hungary, June 1988. Draft submitted for voting to the Members of the International Committee of Legal Metrology.
2. WHO, 1977: The SI for the health professions. Office of Publications, World Health Organisation, Geneva, Switzerland.
3. IAEA, 1987: Absorbed dose determination in photon and electron beams. Technical Report Series No. 277, International Atomic Energy Agency, Vienna, 1987.
4. Urquhart, D.F., Badger, W.S. and Johnson, E.P. [1974]. Standardisation of absorbed dose by means of an aluminium calorimeter. AAEC/E322.
5. Urquhart, D.F., Johnson, E.P. and Badger, W.S. [1978]. The Australian Commonwealth standard of measurement for absorbed radiation dose. AAEC/E455.
6. Sherlock, S.L. Extension of the Commonwealth standard of absorbed dose from Cobalt-60 energy to 25 MV. Australian Physical and Engineering Sciences in Medicine (1986) Vol. 9, No.1.
7. Keithley, 1984. Low Level Measurements. Keithley Instruments, Inc. 28775 Aurora Road, Cleveland, Ohio 44139. Revised Third Edition, Printed June 1984.
8. Zill, D.G., 1982. A first course in differential equations with applications. Second Edition, Prindle, Weber and Schmidt, Boston, U.S.A.
9. Domen, S.R. and Lamperti, P.J., 1974. A heat-loss-compensated calorimeter; theory, design and performance. Journal of Research of the National Bureau of Standards - A. Physics and Chemistry. Vol. 78A, No.5, September-October, 1974.
10. Sherlock, S.L., 1987. Solution of Newtons' law of cooling for a 4-body calorimeter. ANSTO internal publication AP/IN 206.
11. ANSI/IEEE-488-1978. Digital Interface for Programmable Instrumentation. Institute of Electrical and Electronics Engineers, 345 East 47th Street, New York, NY 10017.
12. Du Sautoy, A.R., 1985. The measuring assembly for a primary standard absorbed dose calorimeter. NPL Report RS(EXT)74, October, 1985. National Physical Laboratory, Teddington, Middlesex TW11 OLW, UK.
13. Morrison, R., 1977. Grounding and shielding techniques in instrumentation. Second Edition, A Wiley-Interscience Publication by John Wiley and Sons, New York, 1977. ISBN 0-471-02992-0.
14. Huntley, R.B., 1985. An absorbed dose microcalorimeter. 10th Annual

Conference, Australian Radiation Protection Society, Melbourne, 19-22 August, 1985.

15. Maxwell, J.C., 1868. On Governors. Proc. Roy. Soc. London, 16, 270-282 (1868).

16. Ivanoff, A., 1934. Theoretical Foundations of the Automatic Regulation of Temperature. J. Inst. Fuel, 7(33), 117-138 (1934).

TABLE 1

MATERIALS AND ELEMENTS USED IN CONSTRUCTION

OF THE CALORIMETER ABSORBER

(This table is the revised version of TABLE 2, AAEC/E455)

MATERIAL	COMPOSITION	Mass (mg)	ELEMENT	Mass (mg)
Graphite	C	1669.83	C	1677.70
Aluminium	Aℓ	0.98	H	0.81
Delrin	0.61C + 0.12H + 0.27O	1.05	O	3.03
Karma Wire	0.8Ni + 0.2Cr	9.01	Aℓ	0.98
Thermistors	0.78Fe + 0.22O	0.48	Cr	1.80
Platinum Wire	Pt	0.33	Fe	0.39
Copper Wire	Cu	1.71	Ni	7.21
Solder	0.3Pb + 0.7Sn	0.08	Cu	1.71
Epoxy	0.71C + 0.07H + 0.22O	7.36	Sn	0.06
Acrylic	0.60C + 0.08H + 0.32O	2.68	Pt	0.33
Shellac	0.6C + 0.1H + 0.3O	0.53	Pb	0.02
	Total Mass	1694.04		1694.04

TABLE 2

MEAN ABSORPTION COEFFICIENT $(\bar{\mu}_{en}/\rho)_i$ OF THE ABSORBER IMPURITIES AND THE EFFECTIVE ABSORBER MASS m_o OR A ^{60}Co SOURCE

(This table is the revised version of TABLE 3, AAEC/E455)

COMPONENT			$(\bar{\mu}_{en}/\rho)_i$ at depth (g.cm^{-2}) in graphite (cm^2.g^{-1})			
i	ELEMENT	Mass m_i (mg)	5	7	10	20
C	C	1677.70	.0271	.0271	.0272	.0272
1	H	0.81	.0539	.0539	.0540	.0541
2	O	3.03	.0272	.0272	.0273	.0273
3	Aℓ	0.98	.0268	.0269	.0270	.0271
4	Cr	1.80	.0296	.0302	.0310	.0316
5	Fe	0.39	.0318	.0328	.0335	.0345
6	Ni	7.21	.0343	.0350	.0365	.0377
7	Cu	1.71	.0338	.0345	.0365	.0374
8	Sn	0.06	.0527	.05451	.05704	.06021
9	Pt	0.33	.1541	.1530	.1552	.1620
10	Pb	0.02	.0908	.0938	.0975	.1011
Total Mass m_a (mg): 1694.04						
$\therefore m_o$ (mg)		:	1699.06	1699.34	1699.90	1700.43

where $$m_o = m_c + \sum_{i=j}^{10} \left[(\bar{\mu}_{en}/\rho)_c^i \, m_i \right]$$

TABLE 3

MEAN MASS ATTENUATION COEFFICIENTS $(\bar{\mu}/\rho)_j$ FOR THE CALORIMETER IMPURITY MATERIALS, THE FLUENCE RATIO $\frac{x_o}{x_a}$ AND THE CORRECTION FACTOR k_i

(This table is the revised version of TABLE 4, AAEC/E455)

COMPONENT				$(\bar{\mu}/\rho)_j$ ($cm^2.g^{-1}$) at depth ($g.cm^{-2}$)			
j	Material	$\Delta d_j \rho_j$ ($mg.cm^{-2}$)	ρ_j ($g.cm^{-3}$)	5	7	10	20
C	Graphite		1.80	.0646	.0647	.0647	.0652
1	Aluminium	1.1	2.70	.0632	.0633	.0637	.0640
2	Heater Wires	2.9	8.1	.0707	.0708	.0739	.0746
3	Bonding Material	1.8	1.15	.0710	.0711	.0712	.0717
4	Insulating Material	1.0	1.19	.0710	.0711	.0712	.0717
$\frac{x_o}{x_a} = \exp\left\{\sum_{j=1}^{4} \Delta d_j \, (\bar{\mu}_j - \bar{\mu}_c)\right\}$:				1.000105	1.000105	1.000114	1.000115
From Table 2, $\frac{m_a}{m_o}$:				.9971	.9969	.9966	.9962
$\therefore$ k_i :				.9972	.9970	.9967	.9964

$$\left(k_i = \frac{m_a}{m_o} \cdot \frac{x_o}{x_a}\right)$$

TABLE 4

SUMMARY OF SYSTEM VOLTMETER SPECIFICATIONS

Instrument Type	Range (μV)	Resolution (nV)	Noise (p-p) (nV)	Input Resistance (MΩ)	Temperature Coefficient %	Accuracy %	Reading Rate (s^{-1})	IEEE-488 (1978)
HP 3457	30000	10	-	10^4	.0005	.0012	.48	Yes
HP 3478	30000	100	-	10^4	.0028	.027	2.3	Yes
Keithley 147	30	10	3	1	-	1	-	No
Keithley 181	2000	10	30	10^3	.002	.006	4	Yes

TABLE 5

SUMMARY OF SYSTEM D/A POWER SUPPLY SPECIFICATIONS

Device Number	Function	Output (bits)	LSB	Range	Ripple and Noise	Settling Time (ms)	Max. Current	Compliance Voltage
44429A	VDAC	12	2.5 mV	± 10.23V	2.5 mV rms	100	15 mA	-
44430A	IDAC	12	4 μA	20.47 mA	5 μA rms	100	-	12V

TABLE 6

COMPILATION OF SYSTEM COMPONENTS USED TO CONTROL AND MONITOR THE GRAPHITE MICROCALORIMETER

MANUFACTURER	MODEL NUMBER	FUNCTION	FUNDS SOURCE
Hewlett Packard	86B	Computer	ANSTO
	7440	X-Y Plotter	"
	2225	Printer	"
	9121D	Disc Drive (dual)	"
	3478A	DMM	"
	3497A	Data Acquisitiion Unit	"
	44429A	VDAC	"
	44430A	IDAC (2)	"
	44421A	Relay Multiplexer	"
	82912A	Video Monitor	"
	00085-15002	Plotter ROM	"
	00087-15004	Matrix ROM	"
	00087-15003	I/O ROM	"
	82909A	128K Memory Module	"
	44425A	Isolated Digital Input	"
	3457A	Transfer Standard DMM	Aust.Instit. of Health
Keithley	147	Nanovoltmeter (2)	ANSTO
	181	Nanovoltmeter (3)	Westmead Hospital (2)
Topward	TPS4000	Dual Power Supply	ANSTO
Leeds & Northrop	4756	AC-DC Decade Resistor	"

TABLE 7

DRIFT RATES AND HEATING RATES OF THE URQUHART CALORIMETER DERIVED FROM MEASUREMENTS IN A 6MV BREMSSTRAHLUNG BEAM (VARIAN CLINAC 1800) EACH RADIATION RUN WAS FOLLOWED BY THE CORRESPONDINGLY NUMBERED ELECTRICAL HEATING RUN

HEATING BY 6 MV RADIATION					
RUN NO.	INITIAL DRIFT RATE	FINAL DRIFT RATE	DIFFERENCE	HEATING RATE	$\frac{\text{DIFFERENCE}}{\text{HEATING RATE}}$ %
	($pV.s^{-1}$)	($pV.s^{-1}$)	($pV.s^{-1}$)	($pV.s^{-1}$)	
1	+ 90	+ 203	+ 113	86967	+ 0.13
2	+ 137	+ 60	- 77	86413	- 0.09
3	- 163	- 73	+ 90	86677	+ 0.10
4	+ 790	+ 830	+ 40	78887	+ 0.05
5	- 213	- 93	+ 120	86457	+ 0.14
6	+ 840	+ 523	- 317	87013	- 0.36
7	+ 1020	+ 330	- 690	87070	- 0.79
8	+ 517	+ 240	- 277	87333	- 0.32
9	+ 1573	+ 123	- 1450	86680	- 1.67
10	+ 277	+ 330	+ 53	87137	+ 0.06
MEAN	+ 487	+ 247	- 240	86063	- 0.28
HEATING BY ELECTRICAL MEANS					
1	+ 67	+ 103	+ 37	75740	+ 0.05
2	- 90	+ 43	+ 133	75493	+ 0.18
3	+ 243	+ 580	+ 337	78647	+ 0.43
4	+ 757	+ 803	+ 47	87013	+ 0.05
5	- 43	+ 1020	+ 1063	78440	+ 1.36
6	+ 627	+ 730	+ 103	78837	+ 0.13
7	+ 243	+ 653	+ 410	77503	+ 0.53
8	+ 177	+ 170	- 7	78320	- 0.01
9	+ 230	+ 147	- 83	78077	- 0.11
10	+ 217	+ 307	+ 90	78097	- 0.11
MEAN	+ 243	+ 457	+ 214	78617	+ 0.27

TABLE 8

DRIFT RATES AND HEATING RATES OF THE URQUHART CALORIMETER DERIVED FROM MEASUREMENTS IN A 18MV BREMSSTRAHLUNG BEAM (VARIAN CLINAC 1800) EACH RADIATION RUN WAS FOLLOWED BY THE CORRESPONDINGLY NUMBERED ELECTRICAL HEATING RUN

RUN NO.	INITIAL DRIFT RATE	FINAL DRIFT RATE	DIFFERENCE	HEATING RATE	$\frac{\text{DIFFERENCE}}{\text{HEATING RATE}}$ %
HEATING BY 18 MV RADIATION					
	($pV.s^{-1}$)	($pV.s^{-1}$)	($pV.s^{-1}$)	($pV.s^{-1}$)	
1	- 80	- 220	- 140	104997	- 0.13
2	- 187	- 73	+ 114	105100	+ 0.11
3	+ 250	+ 343	+ 93	105133	+ 0.09
4	+ 243	+ 350	+ 107	105190	+ 0.10
5	- 3	0	+ 3	104810	+ 0.0
6	- 87	- 63	+ 24	104957	+ 0.02
7	- 23	- 63	- 40	105160	- 0.04
8	+ 223	+ 287	+ 64	105293	+ 0.06
9	+ 313	+ 247	- 66	105477	- 0.06
10	- 100	- 43	+ 57	104423	+ 0.05
MEAN	+ 55	+ 77	+ 22	105054	+ 0.02
HEATING BY ELECTRICAL MEANS					
1	- 217	- 343	- 126	96913	- 0.13
2	- 33	- 93	- 60	97043	- 0.06
3	+ 243	+ 160	- 83	96957	- 0.09
4	+ 103	- 37	- 140	96507	- 0.15
5	- 247	- 493	- 246	96103	- 0.26
6	- 67	- 203	- 136	97250	- 0.14
7	- 77	- 163	- 86	97000	- 0.09
8	+ 140	+ 153	+ 13	96863	+ 0.01
9	- 50	- 173	- 123	966536	- 0.13
10	- 97	- 247	- 150	96630	- 0.15
MEAN	- 30	- 143	- 113	96800	- 0.12

TABLE 9

ABSORBED DOSE RATE ($mGy.s^{-1}$) IN GRAPHITE FOR 6 AND 18 MV BREMSSTRAHLUNG RADIATION GENERATED BY A VARIAN CLINAC 1800

RUN NO.	6 MV DOSE RATE ($mGy.s^{-1}$)	18 MV DOSE RATE ($mGy.s^{-1}$)
1	44.82	54.27
2	44.64	54.36
3	44.70	54.35
4	44.50	54.54
5	44.76	54.50
6	44.50	54.11
7	45.17	54.34
8	44.83	54.48
9	44.93	54.54
10	44.94	54.15
$\bar{X}$:	44.78	54.36
S :	.21	.15
$100\ S/(\sqrt{n}\ \bar{X})$	.15%	.09%

Figure 1: Non-scale diagram of Urquhart graphite calorimeter illustrating architecture.

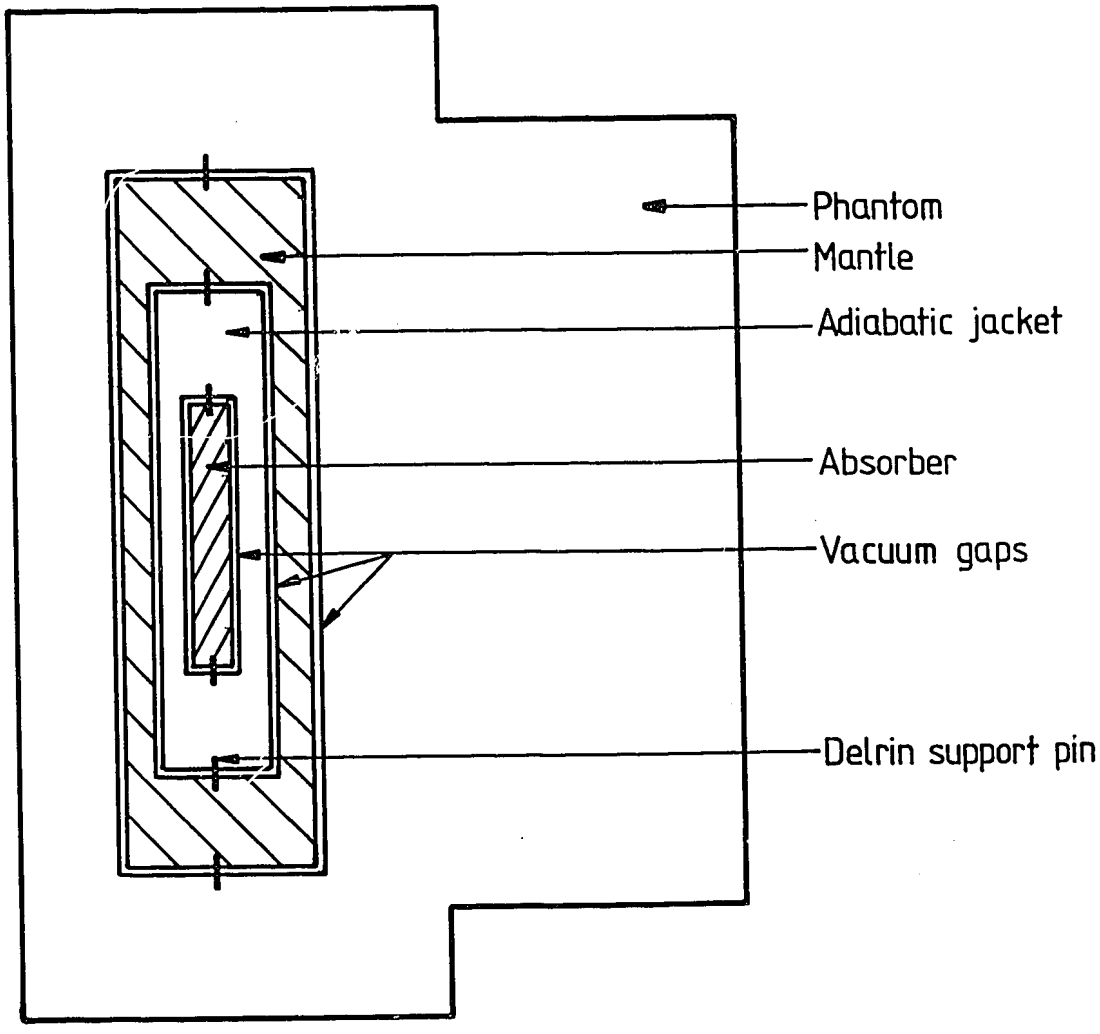

Figure 2: Block Diagram of Calorimeter Control and Monitoring Electronics; Initial System using Keithley 147 Nanovoltmeters

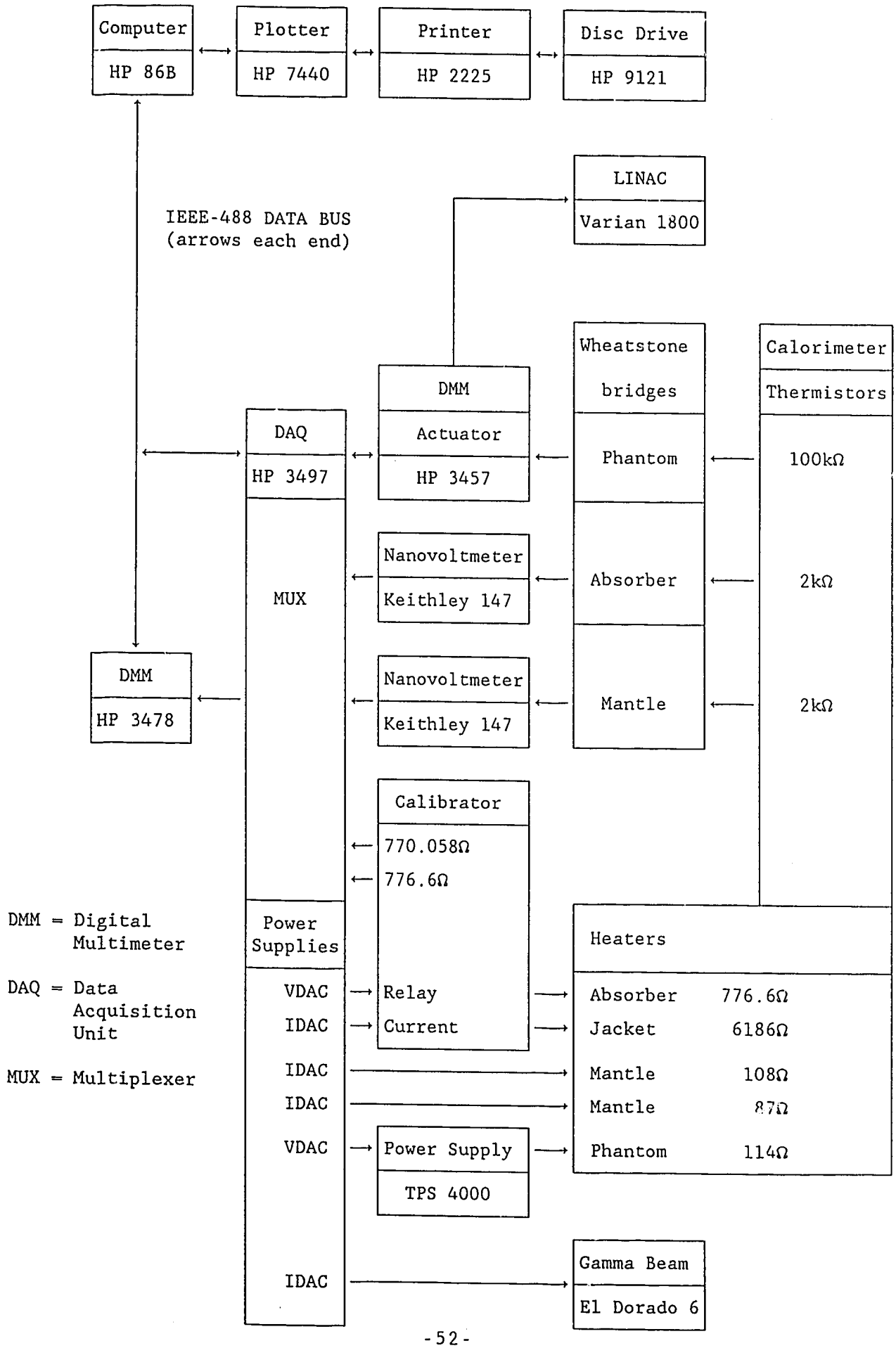

Figure 3: Block Diagram of Calorimeter Control and Monitoring Electronics; Final System using Keithley 181 Nanovoltmeters

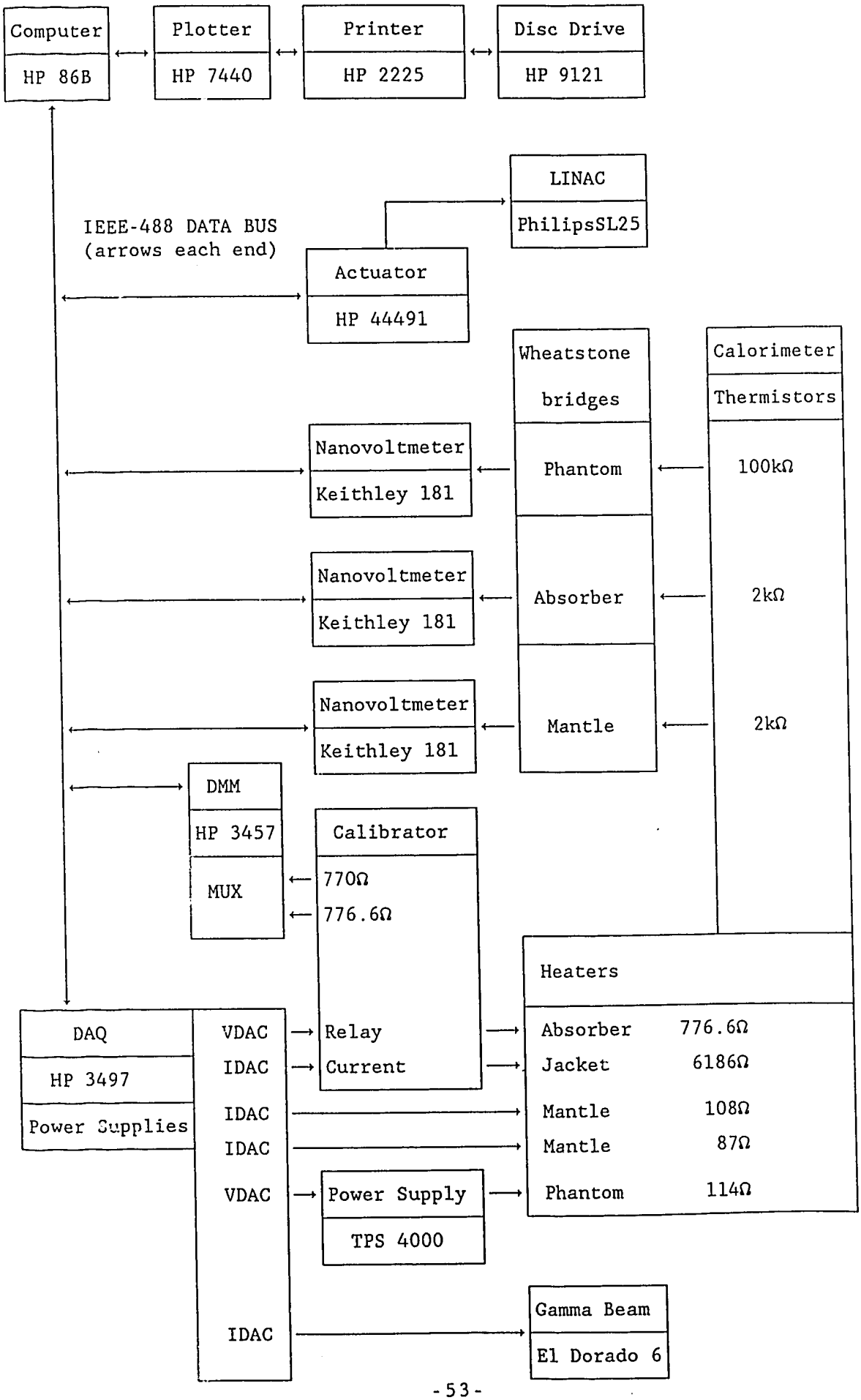

Figure 4: Absorber temperature sensing circuit. Resistors are manganin wound, temperature coefficient < 5 ppm.C^{-1} supplied by Leeds and Northrop.

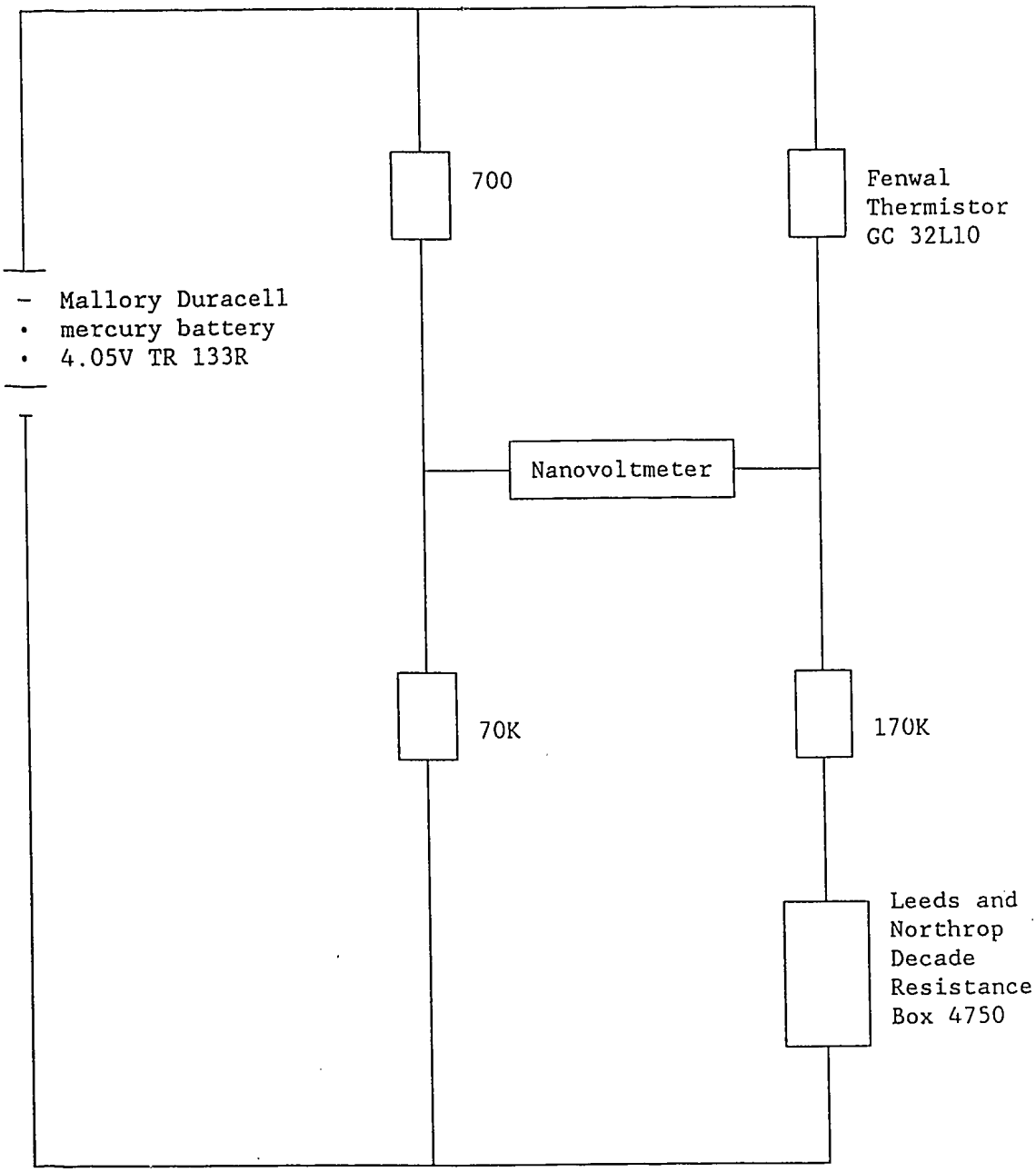

Figure 5: Mantle temperature sensing circuit. Resistors are either manganin (M) or nichrome (N) wound, temperature coefficient < 5 ppm.C^{-1}.

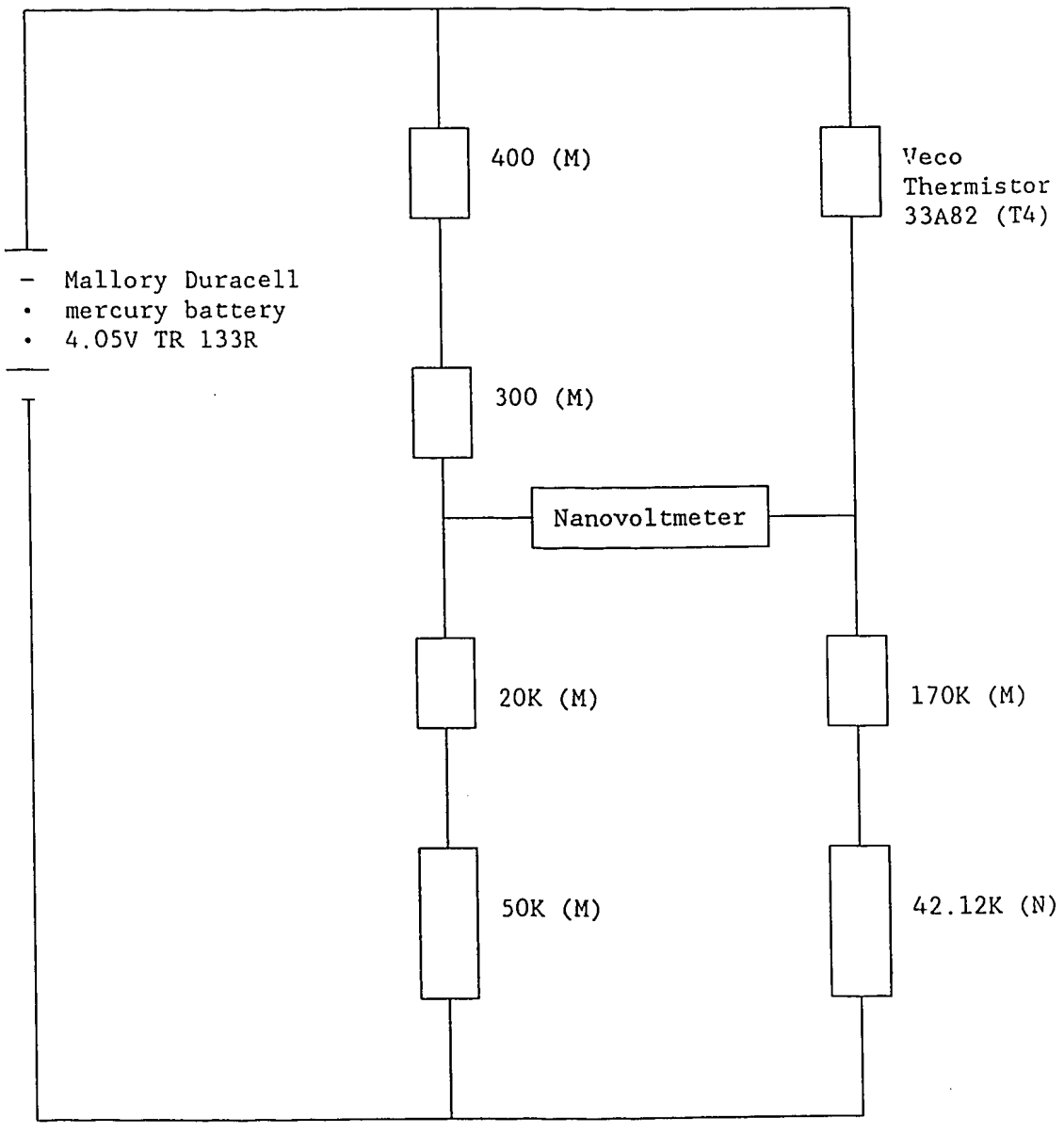

Figure 6: Phantom temperature sensing circuit. Resistors are nichrome (N) wound, temperature coefficient < 5 ppm.C^{-1}.

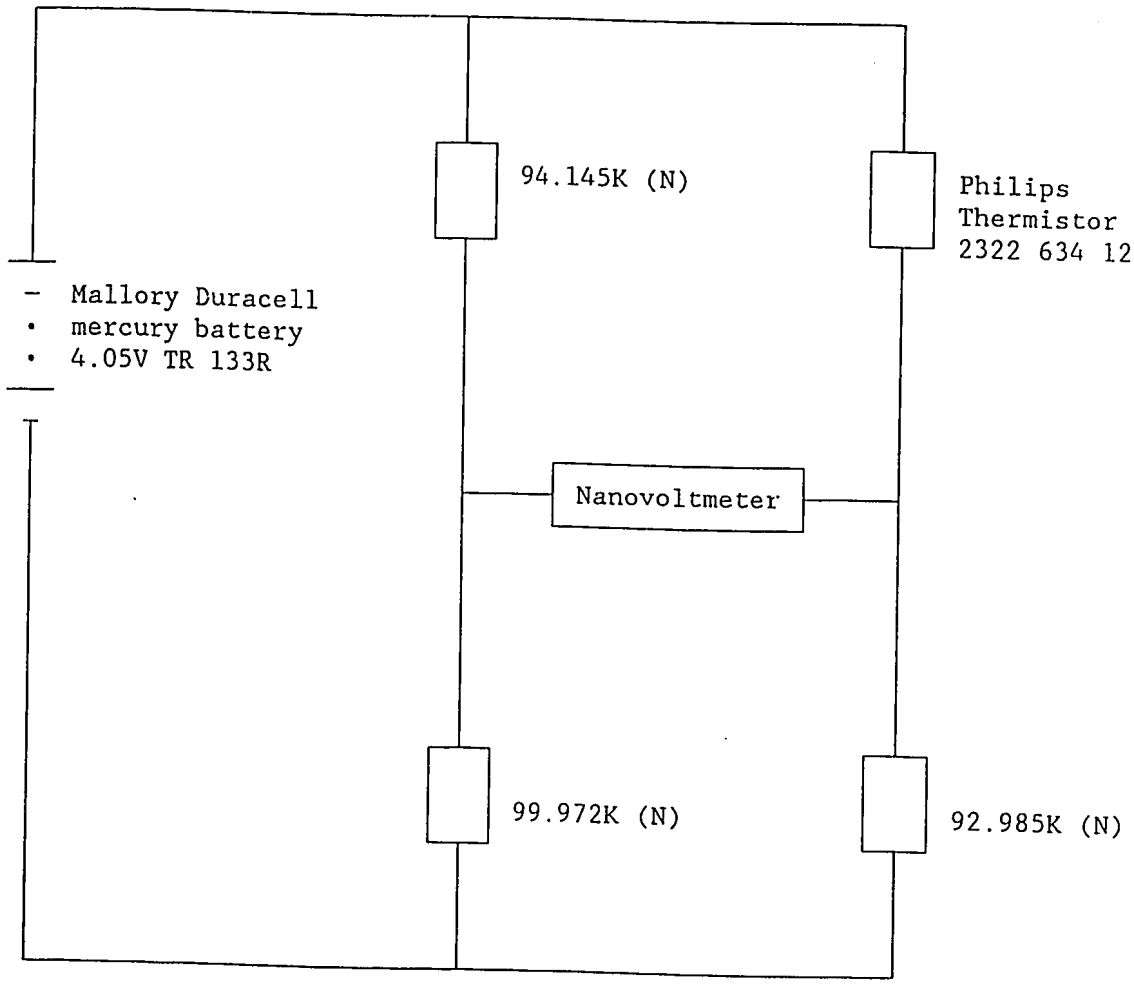

Figure 7: Calibrator circuit. Resistors are wire wound (WW), nichrome (N) or manganin (M). Heater windings 6186Ω and 776.6Ω are epoxy-enamelled Karma wire. The circuit is screened in a die-cast aluminium box.

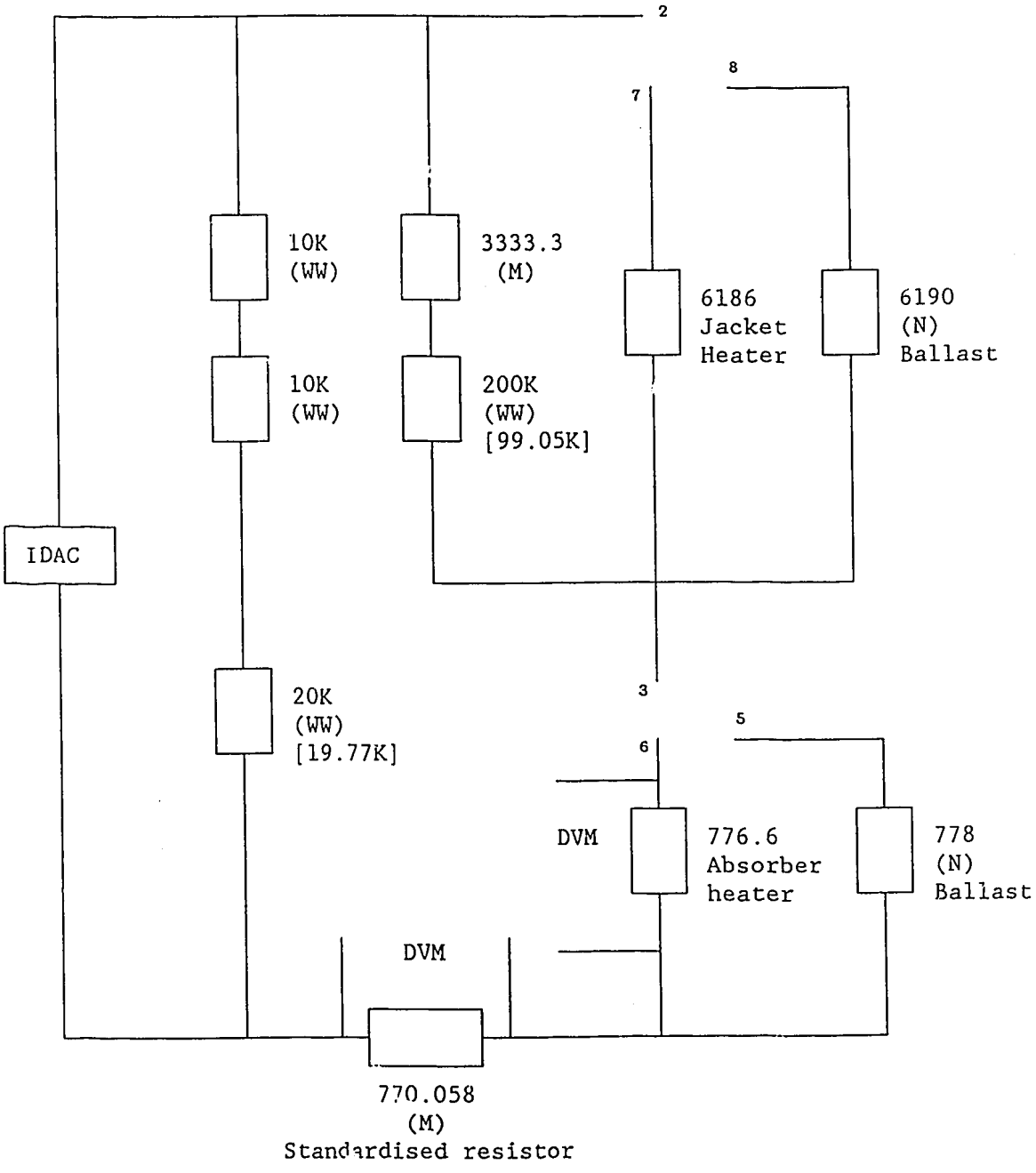

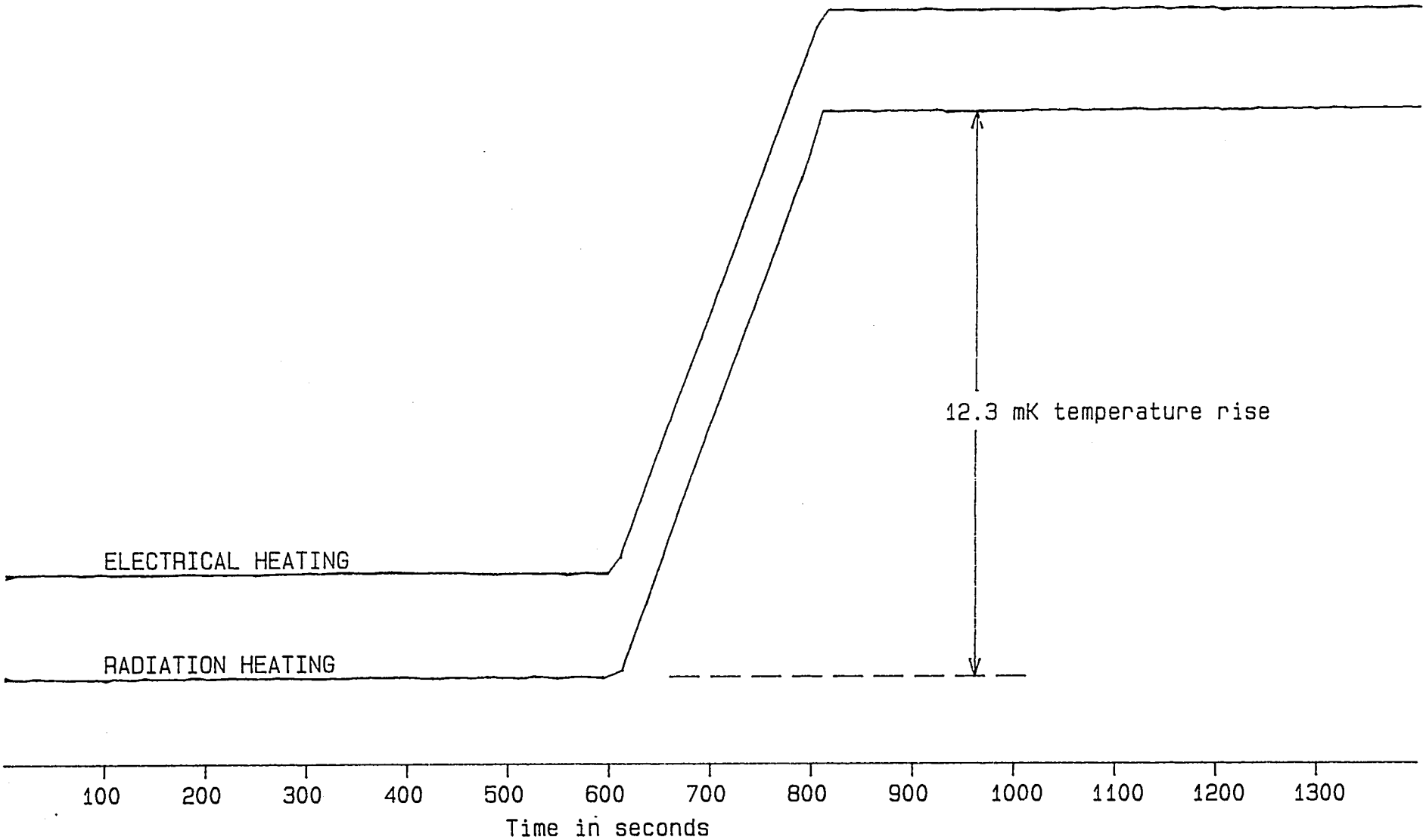

Figure 8: Plot of electrical and radiation heating from measurements at 6 MV on a VARIAN CLINAC 1800. These data correspond to RUN#1 in Table 7. Straight lines have been fitted to and plotted on the drift and heating sections.

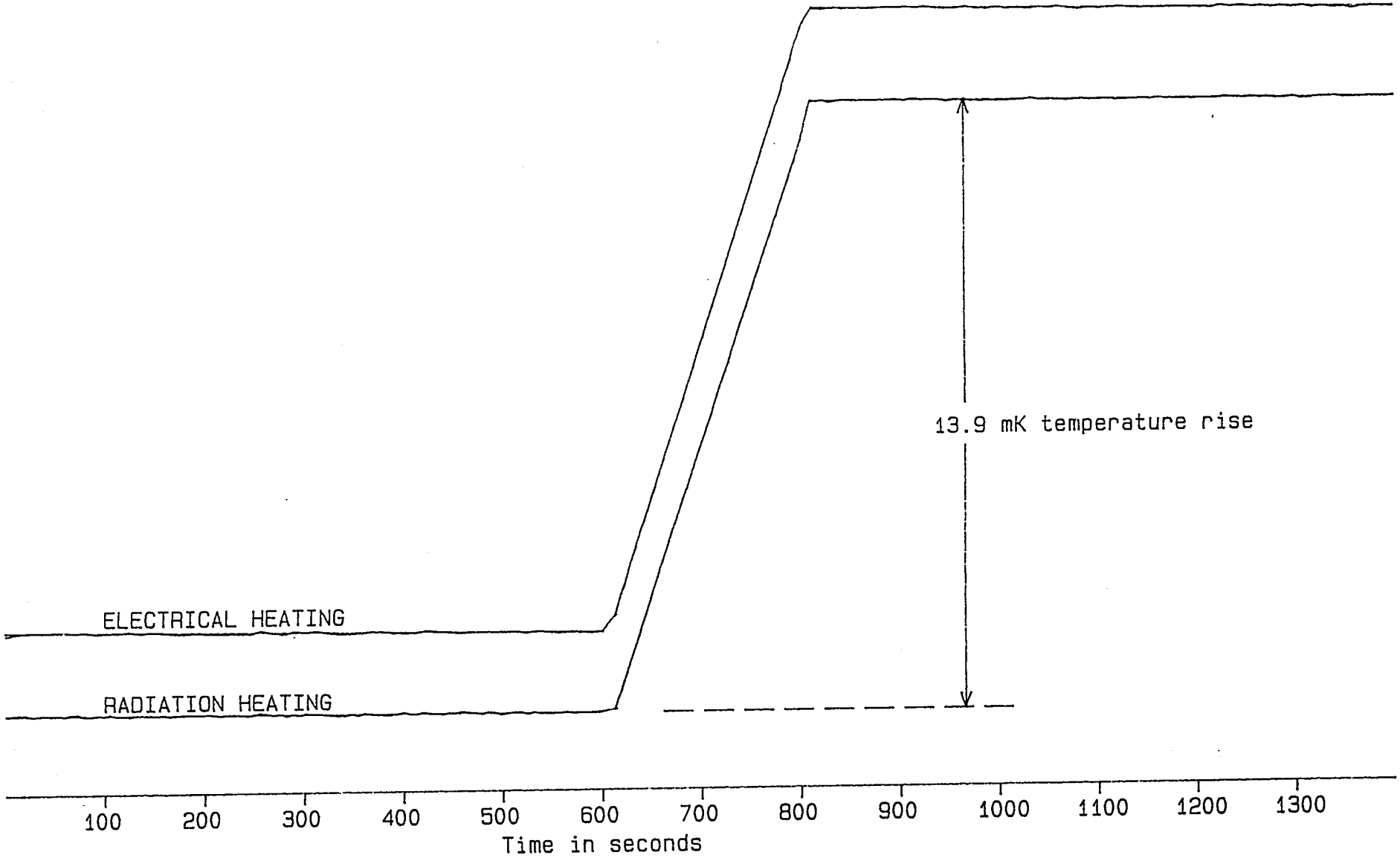

Figure 9: Plot of electrical and radiation heating from measurements at 18 MV on a VARIAN CLINAC 1800. These data correspond to RUN#1 in Table 8. Straight lines have been fitted to and plotted on the drift and heating sections.

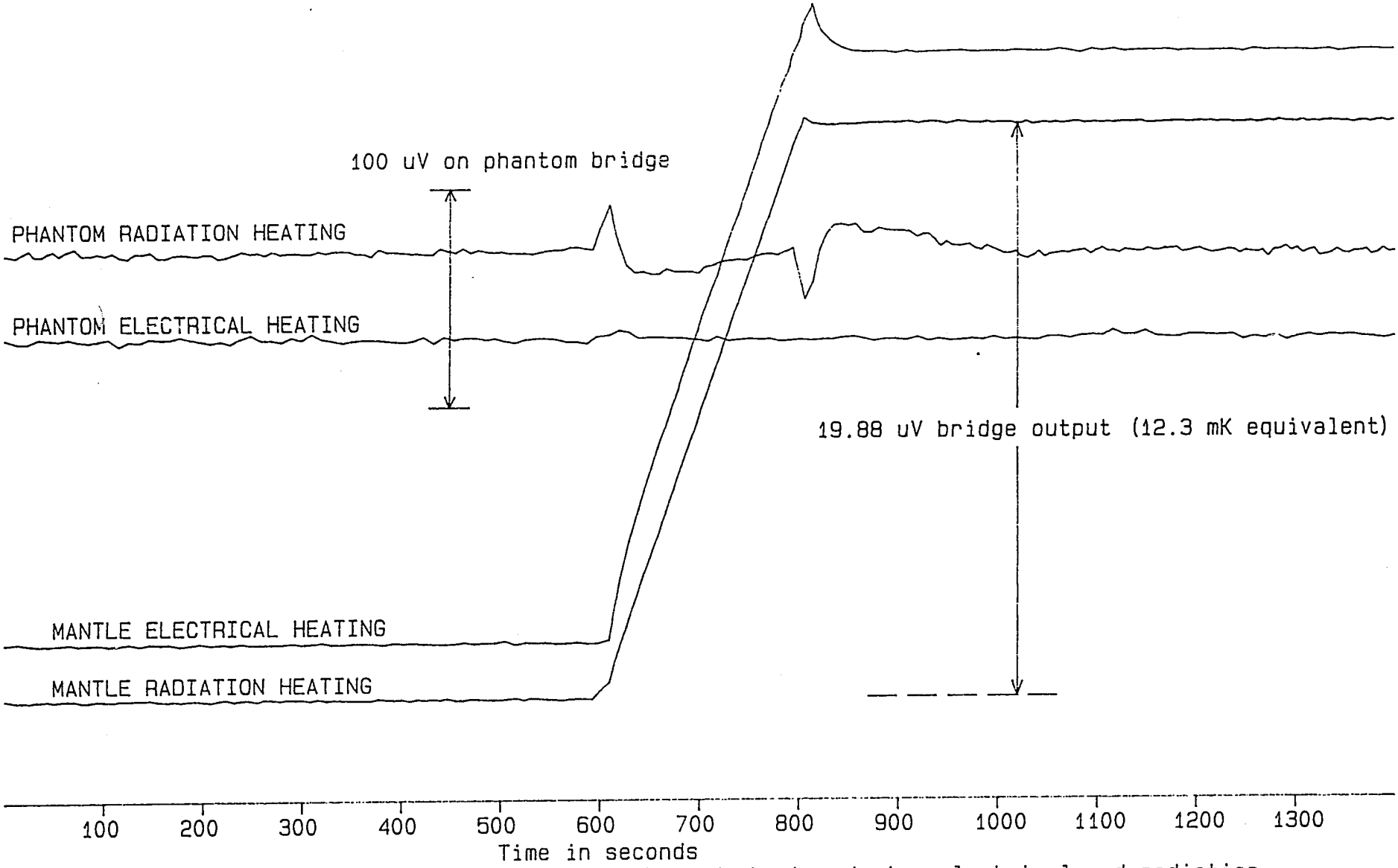

Figure 10: Plot of temperature response of mantle and phantom during electrical and radiation heating at 6 MV on a VARIAN CLINAC 1800. These data were collected at the same time as RUN #1 in Table 7.

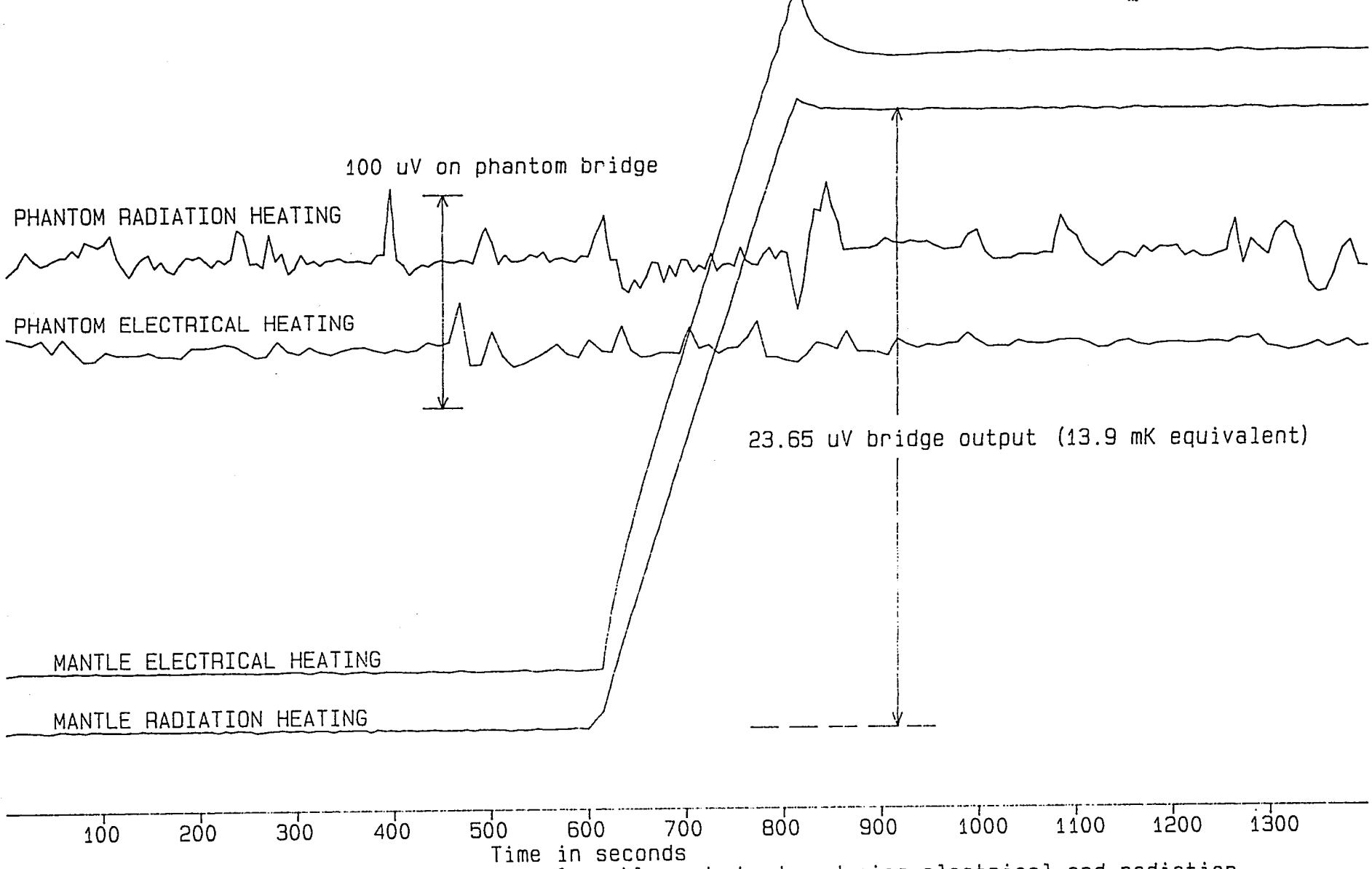

Figure 11: Plot of temperature response of mantle and phantom during electrical and radiation heating at 18 MV on a VARIAN CLINAC 1800. These data were collected at the same time as RUN #1 in Table 8.